Skew-symmetric Nitsche's formulation in isogeometric analysis: Dirichlet and symmetry conditions, patch coupling and frictionless contact

Qingyuan Hu, Franz Chouly, Gengdong Cheng, Stéphane Pierre Alain Bordas

Skew-symmetric Nitsche's formulation in isogeometric analysis: Dirichlet and symmetry conditions, patch coupling and frictionless contact

Qingyuan Hu[a,b], Franz Chouly[c], Gengdong Cheng[a], Stéphane P.A. Bordas[b,c,d,e,*]

[a] *Department of Engineering Mechanics, Dalian University of Technology, Dalian 116024, P.R. China*
[b] *Institute of Computational Engineering, Faculty of Sciences Technology and Communication, University of Luxembourg, Luxembourg*
[c] *Laboratoire de Mathématiques de Besançon - UMR CNRS 6623, Université Bourgogne Franche-Comté, 16 route de Gray, 25030 Besançon cedex, France*
[d] *Institute of Mechanics and Advanced Materials, School of Engineering, Cardiff University, UK*
[e] *Intelligent Systems for Medicine Laboratory, University of Western Australia, Perth, Australia*

Abstract

A simple skew-symmetric Nitsche's formulation is introduced into the framework of isogeometric analysis (IGA) to deal with various problems in small strain elasticity: essential boundary conditions, symmetry conditions for Kirchhoff plates, patch coupling in statics and in modal analysis as well as Signorini contact conditions. For linear boundary or interface conditions, the method is parameter-free. For contact conditions, skew-symmetric Nitsche remains stable and accurate for a wide range of the stabilization parameter. Several numerical tests are performed to illustrate its accuracy, stability and convergence performance. We investigate particularly the effects introduced by Nitsche's coupling, including the convergence performance and condition numbers in statics as well as the extra "outlier" frequencies and corresponding eigenmodes in structural dynamics. We present the block test and Hertz test showing that skew-symmetric Nitsche's formulation is a suitable approach to simulate contact problems in IGA.

Keywords: isogeometric, Nitsche, parameter-free, contact, patch coupling, boundary condition.

1. Introduction

The key concept in isogeometric analysis (IGA) [1] consists in using non-uniform rational B-splines (NURBS) as basis functions to approximate both the geometry and the unknown physical fields. The mathematical foundations of IGA are developed in [2], and a recent overview is given in [3]. Contrary to classical Lagrange basis functions usually adopted in the finite element method (FEM), NURBS in IGA have the ability to exactly describe geometries: thus, no geometrical approximation error is introduced.

*Corresponding author
Email addresses: huqingyuan@mail.dlut.edu.cn (Qingyuan Hu), franz.chouly@univ-fcomte.fr (Franz Chouly), chenggd@dlut.edu.cn (Gengdong Cheng), stephane.bordas@alum.northwestern.edu (Stéphane P.A. Bordas)

Moreover NURBS are widely adopted in commercial computer-aided design (CAD) packages, and this CAD data can directly be used to construct approximations. In boundary element method (BEM), this translates into the ability to solve directly from the field variables at the control points defining the geometry [4, 5, 6, 7, 8, 9, 10, 11]. In FEM, a 3D parameterization of the volume is still necessary [12, 13], except when solving shell-like problems [14, 15, 16, 17, 18]. The present paper focuses on two following issues. One first issue in IGA is related to boundary conditions, especially essential boundary conditions. Indeed, since NURBS are non-interpolatory, enforcing boundary conditions and constraints cannot be done as simply as in Lagrange FEM: they require tackling difficulties which are similar to those encountered in meshless methods [19] and implicit/immersed boundary methods [20, 21]. One second issue in IGA comes from patch coupling and interface conditions: for complex geometries, patch-wise CAD modeling is necessary, and transmission conditions need to be satisfied. The same also arises when gluing heterogeneous materials.

Various methods already exist to treat boundary or interface conditions weakly, that have been firstly designed for instance in the FEM context, and that are applicable, or have already been applied, for IGA. The most widespread ones are the penalty method, mixed/mortar methods and Nitsche's method. The penalty method [22, 23] is simple but not consistent, and the value of the penalty parameter has to be chosen with great care to achieve the best balance between accuracy and stability. As a matter of fact, if the penalty parameter is chosen too small the boundary or interface conditions are imposed inaccurately, whereas if it is chosen much larger than needed the penalized problem becomes ill-conditioned. Mixed methods for boundary conditions [24] introduce a Lagrange multiplier, which is an additional variable that represents the boundary stress, and that allows to take into account weakly the essential boundary condition in a consistent way. This leads to a weak problem that has a saddle-point structure. For patch-coupling, the original mortar method [25, 26] has been reformulated later as a mixed/dual Lagrange multiplier method (see, e.g., [27, 28] for FEM and [29] for IGA). Mortar methods, when carefully designed, are consistent, stable and optimally accurate. Moreover the newly introduced Lagrange multipliers have a clear meaning: they are the stresses needed to enforce the continuity of the displacements. Mortar techniques have been applied as well with success to contact problems [30, 31, 32, 33, 34, 35]. However extra degrees of freedoms (DoFs) are introduced and an inf-sup condition must be fulfilled in order to ensure stability and optimal convergence, for which care is needed to build the dual space of Lagrange multipliers.

Nitsche's method was originally proposed by J. Nitsche [36, 37] to impose weakly essential boundary conditions and more recently has regained popularity to deal with interface conditions with non-conforming discretizations (see, e.g., [38, 39, 40]). Nowadays Nitsche's method has also found a number of natural

applications in IGA [41, 42, 43, 44, 45, 46]. Nitsche's formulation makes use of appropriate *conjugate pair* such as displacement–force or rotation–moment, in such a way that the method remains both primal (no extra DoFs) and consistent. By the way, there is no need to fulfill an inf-sup condition. However, standard (symmetric) Nitsche's method includes an extra term that penalizes the boundary/interface conditions, and which is necessary for stability and optimal accuracy. In this term an additional numerical parameter, the *stabilization parameter*, needs to be fixed above a given threshold for this purpose. For simple problems and numerical methods (such as Lagrange FEM of low-order), a direct estimation of the aforementioned threshold can be effectuated, but for more realistic problems and less standard numerical methods, an *a priori* knowledge of this threshold is harder to achieve. Then one common approach to estimate the stabilization parameter is to solve a generalized eigenvalue problem along the target boundary/interface: see, e.g., [41, 42, 43]. Of course, an alternative technique remains to estimate the stabilization parameter, based on e.g. Young's modulus, mesh sizes and other problem-dependent parameters [40, 47, 48]. This difficulty can be circumvented by using the penalty-free (skew-symmetric) variant of Nitsche's method, such as in [49, 50, 51, 52, 53].

In this paper we present a simple and systematic procedure to derive, for various boundary and interface conditions, a family of Nitsche's formulations that have different symmetry properties and different degrees of dependency. This family is indexed by the *Nitsche parameter* θ. We then focus on the variant known as the skew-symmetric Nitsche method, that corresponds to the value $\theta = -1$. This method can be parameter-free when dealing with linear boundary or interface conditions, and reveals to be very robust with respect to the Nitsche parameter for non-linear boundary conditions such as contact. Let us mention that in the context of standard FEM, the skew-symmetric method has been successfully applied to contact [54, 55, 56]. Furthermore in IGA there is already one contribution on the skew-symmetric Nitsche method for enforcing Dirichlet boundary conditions and patch coupling for thin shell problems [57]. In this contribution we perform numerical experiments for different situations, particularly we study how Nitsche's multi-patch coupling can affect the accuracy, the convergence rates, and the condition numbers. Moreover, in modal analysis, literature [58, 59] shows that some outlier frequencies appear due to the discretization of the continuous problem. This "outlier" phenomenon is also captured in multi-patch cases using the mortar method [60]. Here we study this issue of the "outlier" frequencies and corresponding eigenmodes, in the context of Nitsche's method. Finally to our knowledge Nitsche's method has never been applied in IGA for contact conditions, and we show how to implement Nitsche's formulation for contact problems, and how it performs in this case.

The outline of this paper is as follows. In Section 2 the concept and notations of IGA are introduced, the critical differences between Lagrange-based FEM and NURBS-based IGA are also explained. In Section 3 we introduce the Nitsche-based formulations for boundary/interface conditions, starting from an abstract setting. In Section 4 various numerical tests are performed and we reach conclusions in Section 5.

2. Brief introduction to isogeometric analysis

Bivariate NURBS basis functions $R_A(\xi,\eta),(A=1,\cdots,nm)$ are often adopted in IGA to generate surfaces, they are constructed by weights w_A and the tensor product of two sets of univariate B-spline basis functions $N_{i,p}(\xi),(i=1,\cdots,n)$ and $N_{j,q}(\eta),(j=1,\cdots,m)$, where p and q are orders of the B-spline basis functions in direction ξ and η respectively. One set of B-spline basis functions can be calculated from one given knot vector recursively [61]. By the help of NURBS basis functions, the desired surface is modeled as

$$\boldsymbol{x}=\sum_{A}^{nm} R_A \boldsymbol{x}_A,$$

where $\boldsymbol{x}_A(x,y,z)$ denote positions of the control points. Following the "iso" concept, the physical field is interpolated by the same set of NURBS basis functions as

$$\mathbf{u}=\sum_{A}^{nm} R_A \mathbf{u}_A,$$

where $\mathbf{u}_A$ are the control point variables. According to [62] the spline spaces used for the geometry and the physical field can be chosen and adapted independently, which is known as the Geometry-Independent Field approximaTion (GIFT) and brings more flexibility in the field approximation when preserving geometric exactness and tight CAD integration. However this research is restricted to IGA.

In Figure (1) some differences between Lagrange FEM and IGA are illustrated. On the left side the curved model is discretized into four traditional finite elements, all these four elements use the same set of Lagrange basis functions from the parent coordinate. Since the Lagrange basis functions are interpolated at both ends, the FEM node are located at the geometry, and it is clear that discrete errors are introduced in the FEM mesh. On the right side, the curved model is described exactly by only one isogeometric element of order $p=2$ with three control points. The adopted NURBS basis functions could have a desired higher order derivatives up to C^{p-1}. It is noticed that except for the two control points on both ends, the middle control point is not located at the model, which is owing to its corresponding non-interpolated basis function. In more general cases, we may consider that the control points that define the boundary/interface are not

interpolated, this brings difficulties in directly manipulating the control variables attached to these control points when dealing with boundary and interface conditions. In the next section we are going to introduce Nitsche's formulation to impose various boundary/interface conditions weekly.

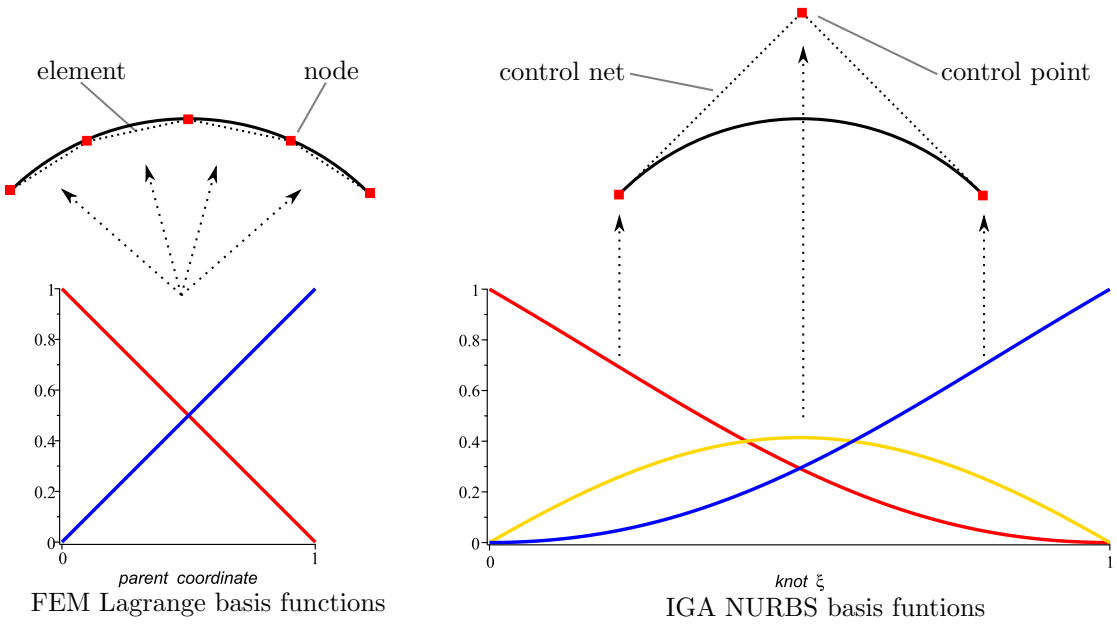

Figure 1: 1D element discretization: Lagrange basis function based FEM (left) and NURBS basis functions based IGA (right). In IGA due to the non-interpolated NURBS basis function (yellow), the middle control point is not located at the geometry.

3. Nitsche's formulation for boundary/interface conditions

We present first Nitsche's method within an abstract setting, and then apply this framework to recover various well-known Nitsche-based discretizations, for a wide range of problems in computational mechanics. Note that for linear boundary and interface conditions, discretized with finite elements, a general presentation can be found in, e.g., [37, 38, 39]. We will consider a whole family of Nitsche's methods indexed by a real value, that we will call the *Nitsche parameter* $\theta \in \mathbb{R}$, and we will pay attention to the skew-symmetric variant, recovered when $\theta = -1$.

3.1. Abstract setting

Consider in the following we want to compute a field $\mathbf{u} : \Omega \to \mathbb{R}^d$ $(d \geq 1)$, for instance a displacement, that is solution to a given set of partial differential equations with prescribed boundary/interface conditions. We will denote by $\mathbf{v}$ an arbitrary test function, that can represent the virtual displacement. We will denote

by Γ either a portion of the boundary of Ω or an interface that subdivides Ω into two subdomains. Two main ingredients are necessary to build a Nitsche-based formulation.

The first ingredient is a Green formula (inspired by Theorem 5.8 in [23]), that we provide below in an abstract setting:

$$a(\mathbf{u},\mathbf{v}) - \langle \boldsymbol{\tau}(\mathbf{u}), \mathbf{B}\mathbf{v}\rangle_\Gamma = L(\mathbf{v}), \tag{1}$$

where $a(\cdot,\cdot)$ is a bilinear form (the internal work), $\langle\cdot,\cdot\rangle_\Gamma$ is an appropriate duality product for functions on Γ (the boundary/interface work), and $L(\cdot)$ a linear form (the work of external loads). The linear operator $\mathbf{B}$ is a trace-like operator: for instance $\mathbf{B}\mathbf{v}$ can be the value of $\mathbf{v}$ on the boundary, or of its normal component if $\mathbf{v}$ is a vector field. The dual quantity $\boldsymbol{\tau}(\mathbf{u})$ is to be defined for each application, and is generaly related to the boundary/interface stress (if $\mathbf{u}$ is a displacement). We can call $\boldsymbol{\tau}(\mathbf{u})$ and $\mathbf{B}\mathbf{v}$ a *conjugate pair*. We suppose that both $\boldsymbol{\tau}(\mathbf{u})$ and $\mathbf{B}\mathbf{v}$ can be represented at almost every point of the boundary as vectors of dimension k ($1 \leq k \leq d$), $\boldsymbol{\tau}(\mathbf{u}) : \Gamma \to \mathbb{R}^k$, $\mathbf{B}\mathbf{v} : \Gamma \to \mathbb{R}^k$.

The second ingredient is a reformulation of the boundary/interface conditions as follows:

$$\boldsymbol{\tau}(\mathbf{u}) = [\boldsymbol{\tau}(\mathbf{u}) - \gamma(\mathbf{B}\mathbf{u} - \bar{\mathbf{B}})]_S, \tag{2}$$

where $\gamma > 0$ is a *stabilization parameter*, $\bar{\mathbf{B}}$ is a known quantity, and $[\cdot]_S$ is the projection onto S, a closed convex set of $\mathbb{R}^k$.

The path to follow to get a Nitsche-based discretization is then provided by application of the steps described below (which are mathematical valid only for sufficiently smooth fields $\mathbf{u}$ and $\mathbf{v}$):

1. Apply the following decomposition

$$\mathbf{B}\mathbf{v} = -\frac{1}{\gamma}(\theta\boldsymbol{\tau}(\mathbf{v}) - \gamma\mathbf{B}\mathbf{v}) + \frac{\theta}{\gamma}\boldsymbol{\tau}(\mathbf{v}).$$

2. Insert it into (1), which yields

$$a(\mathbf{u},\mathbf{v}) - \frac{\theta}{\gamma}\langle\boldsymbol{\tau}(\mathbf{u}),\boldsymbol{\tau}(\mathbf{v})\rangle_\Gamma + \frac{1}{\gamma}\langle\boldsymbol{\tau}(\mathbf{u}),(\theta\boldsymbol{\tau}(\mathbf{v}) - \gamma\mathbf{B}\mathbf{v})\rangle_\Gamma = L(\mathbf{v}).$$

3. Inject condition (2) into the above formula, so as to impose it weakly

$$a(\mathbf{u},\mathbf{v}) - \frac{\theta}{\gamma}\langle\boldsymbol{\tau}(\mathbf{u}),\boldsymbol{\tau}(\mathbf{v})\rangle_\Gamma + \frac{1}{\gamma}\langle[\boldsymbol{\tau}(\mathbf{u}) - \gamma(\mathbf{B}\mathbf{u} - \bar{\mathbf{B}})]_S,(\theta\boldsymbol{\tau}(\mathbf{v}) - \gamma\mathbf{B}\mathbf{v})\rangle_\Gamma = L(\mathbf{v}).$$

The above formula may have no meaning at the continuous level, but becomes meaningful once all the fields are discretized, and then we obtain the Nitsche-based formulation below

$$A_\theta(\mathbf{u}^h, \mathbf{v}^h) + \frac{1}{\gamma}\langle [P_1(\mathbf{u}^h) + \gamma\bar{\mathbf{B}}]_S, P_\theta(\mathbf{v}^h)\rangle_\Gamma = L(\mathbf{v}^h), \tag{3}$$

with the notations

$$A_\theta(\mathbf{u}^h, \mathbf{v}^h) := a(\mathbf{u}^h, \mathbf{v}^h) - \frac{\theta}{\gamma}\langle \boldsymbol{\tau}(\mathbf{u}^h), \boldsymbol{\tau}(\mathbf{v}^h)\rangle_\Gamma,$$

and

$$P_\theta(\mathbf{v}^h) := \theta\boldsymbol{\tau}(\mathbf{v}^h) - \gamma\mathbf{B}\mathbf{v}^h.$$

An important case to consider is when boundary/interface conditions are linear, which means that $S = \mathbb{R}^k$ in (2) and so the projection operator is merely the identity. Then (3) reads

$$A_\theta(\mathbf{u}^h, \mathbf{v}^h) + \frac{1}{\gamma}\langle P_1(\mathbf{u}^h) + \gamma\bar{\mathbf{B}}, P_\theta(\mathbf{v}^h)\rangle_\Gamma = L(\mathbf{v}^h),$$

and, after re-ordering and simplifications we arrive at

$$a(\mathbf{u}^h, \mathbf{v}^h) - \theta\langle \mathbf{B}\mathbf{u}^h, \boldsymbol{\tau}(\mathbf{v}^h)\rangle_\Gamma - \langle \boldsymbol{\tau}(\mathbf{u}^h), \mathbf{B}\mathbf{v}^h\rangle_\Gamma + \gamma\langle \mathbf{B}\mathbf{u}^h, \mathbf{B}\mathbf{v}^h\rangle_\Gamma = L(\mathbf{v}^h) - \langle \bar{\mathbf{B}}, \theta\boldsymbol{\tau}(\mathbf{v}^h) - \gamma\mathbf{B}\mathbf{v}^h\rangle_\Gamma. \tag{4}$$

When $\theta = 1$, we recover the well-known formulation presented for instance in [37, 38, 39].

Remark 1. *The Nitsche parameter θ allows to select some variants of the Nitsche formulation, that yield different theoretical properties and different degrees of dependency w.r.t. the stabilization parameter γ:*

- *for $\theta = 1$, the standard symmetric Nitsche's method is obtained, that can be derived from an energy functional, and in which a suitable choice for γ is necessary in order to recover well-posedness and optimal accuracy;*
- *for $\theta = 0$, some terms are canceled and we obtain the simple formulation*

  $$a(\mathbf{u}^h, \mathbf{v}^h) - \langle [P_1(\mathbf{u}^h) + \gamma\bar{\mathbf{B}}]_S, \mathbf{B}\mathbf{v}^h\rangle_\Gamma = L(\mathbf{v}^h),$$

  that is prone to extensions for large elastic transformations [63];
- *for $\theta = -1$, the skew-symmetric Nitsche method is obtained, see e.g., [64, 49, 51] for linear boundary*

conditions and [56, 65] for contact conditions. Stability and optimal convergence are ensured whatever is the value of $\gamma > 0$. It is highlighted that for linear boundary/interface conditions, the stability parameter can even be chosen as $\gamma = 0$, resulting in a parameter-free formulation.

When Nitsche formulation is combined with finite elements, stability and optimal accuracy can be proved: see, e.g., [37, 66, 38, 39] for the complete mathematical analysis in the linear setting, and [56] for contact. For this purpose, the stabilization parameter γ should scale as h^{-1}, where h is the size of the elements, and be chosen above a given threshold $Ch^{-1} > 0$. The constant C in this threshold comes from the application of a trace-inverse inequality that allows to bound locally the boundary/interface flux by the energy norm. This constant C depends on 1) some physical constants such as the Young modulus and 2) the polynomial order of the finite element space. In the skew-symmetric case $\theta = -1$, the condition $\gamma \geq Ch^{-1}$ can be relaxed, and it suffices to take $\gamma > 0$, or even $\gamma = 0$ for linear boundary/interface conditions ("penalty-free" variant). A complete mathematical analysis for $(\theta, \gamma) = (-1, 0)$ can be found in, e.g., [49] for Poisson's problem and FEM setting. The same results as above can be expected for the IGA setting though no numerical analysis has been provided to the best of our knowledge. See however [43] for an heuristics to set γ in the symmetric case $\theta = 1$.

In the remaining part of this paper, we will focus on the skew-symmetric variant $\theta = -1$, but numerical tests with the symmetric variant $\theta = 1$ are also performed for comparison purposes.

3.2. Nitsche for boundary conditions

We illustrate how the above framework can be applied to deal with various boundary conditions, thus the case $\Gamma \subset \partial\Omega$. The unit normal vector on Γ pointing outward of Ω is denoted by $\boldsymbol{n}$.

3.2.1. Dirichlet boundary conditions in small strain elasticity

Consider an elastic body, with the small strain assumption, that is is subjected to body forces $\boldsymbol{b}$, and surface loads $\bar{\boldsymbol{t}}$ along a Neumann boundary $\Gamma_N \subset \partial\Omega$. The corresponding governing equations read

$$\begin{aligned} -\nabla \cdot \boldsymbol{\sigma}(\mathbf{u}) &= \boldsymbol{b} \qquad \text{in } \Omega, \\ \boldsymbol{\sigma}(\mathbf{u})\boldsymbol{n} &= \bar{\boldsymbol{t}} \qquad \text{on } \Gamma_N, \end{aligned}$$

where $\nabla\cdot$ is the divergence operator for vector-valued functions, and $\boldsymbol{\sigma}$ is the Cauchy stress tensor. The corresponding weak form reads

$$a(\mathbf{u}, \mathbf{v}) - \int_\Gamma \boldsymbol{\sigma}(\mathbf{u})\boldsymbol{n} \cdot \mathbf{v}\, ds = L(\mathbf{v}), \tag{5}$$

where

$$a(\mathbf{u},\mathbf{v}) := \int_\Omega \boldsymbol{\sigma}(\mathbf{u}) : \boldsymbol{\epsilon}(\mathbf{v})\, d\mathbf{x}, \quad L(\mathbf{v}) := \int_\Omega \mathbf{b}\cdot\mathbf{v}\, d\mathbf{x} + \int_{\Gamma_N} \bar{\mathbf{t}}\cdot\mathbf{v}\, ds, \tag{6}$$

and where $\boldsymbol{\epsilon}(\cdot)$ is the small strain tensor. As a result we recover a particular case of (1). Suppose one needs to impose in (5) an essential boundary condition on Γ as illustrated in Figure 2

$$\mathbf{u} = \bar{\mathbf{u}} \qquad \text{on } \Gamma.$$

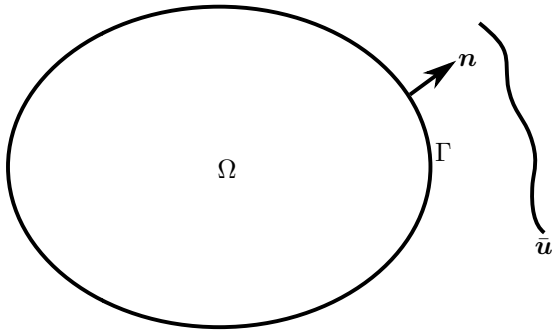

Figure 2: Dirichlet boundary condition: the displacement is equal to $\bar{\mathbf{u}}$ on Γ.

With the choice

$$\mathbf{B}\mathbf{u} = \mathbf{u}, \quad \boldsymbol{\tau}(\mathbf{u}) = \boldsymbol{\sigma}(\mathbf{u})\boldsymbol{n}, \quad \bar{\mathbf{B}} = \bar{\mathbf{u}}, \quad S = \mathbb{R}^d,$$

we obtain from (4) the following Nitsche-based formulation

$$\begin{aligned} & a(\mathbf{u}^h,\mathbf{v}^h) - \theta\int_\Gamma \mathbf{u}^h\cdot\left(\boldsymbol{\sigma}(\mathbf{v}^h)\boldsymbol{n}\right)\, ds - \int_\Gamma \left(\boldsymbol{\sigma}(\mathbf{u}^h)\boldsymbol{n}\right)\cdot\mathbf{v}^h\, ds + \gamma\int_\Gamma \mathbf{u}^h\cdot\mathbf{v}^h\, ds \\ = \quad & L(\mathbf{v}^h) - \theta\int_\Gamma \bar{\mathbf{u}}\cdot\left(\boldsymbol{\sigma}(\mathbf{v}^h)\boldsymbol{n}\right)\, ds + \gamma\int_\Gamma \bar{\mathbf{u}}\cdot\mathbf{v}^h\, ds. \end{aligned} \tag{7}$$

Setting $\theta = -1$ and $\gamma = 0$, the penalty-free variant [49, 44, 51] is recovered.

3.2.2. Symmetry conditions for Kirchhoff-Love plate

Thanks to the higher order continuity properties of NURBS basis functions, there is a regained interest to discretize thin-walled structures using Kirchhoff-Love theory. However due to the absence of rotational DoFs, additional effort is needed to apply rotational boundary conditions. For this fourth-order problem, it is convenient to express the boundary conditions in local coordinates, as illustrated in Figure (3). Also, the

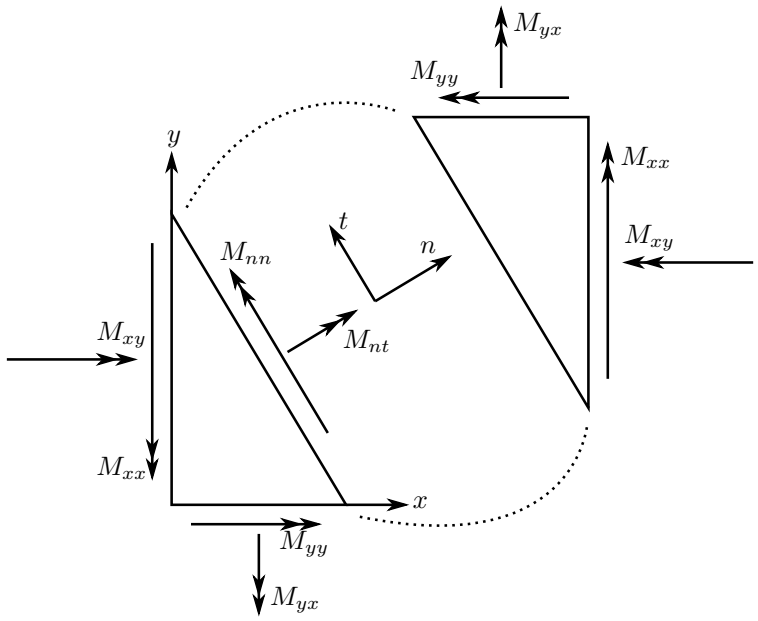

Figure 3: The directions of bending moments in Cartesian coordinate system (x, y) and local system (n, t).

corresponding weak form for Kirchhoff-Love plate reads

$$a(u, v) - \int_\Gamma M_{nn}(u)(-v_{,n})\, ds = L(v), \tag{8}$$

where u is the deflection and v the corresponding virtual quantity, n and t indicate the outward normal direction and tangential direction respectively, $M_{nn}(u)$ is the normal component of the moment tensor ($\boldsymbol{M}(u) = -\mathcal{C} : \nabla^2 u$, where $\mathcal{C}$ is the constitutive fourth-order tensor) and $v_{,n} = (\nabla v) \cdot \boldsymbol{n}$. In this case the bilinear and linear form read (see, e.g., [67] for a more general formulation)

$$a(u, v) := -\int_\Omega \boldsymbol{M}(u) : (\nabla^2 v)\, d\mathbf{x}, \quad L(v) := \int_\Omega F\, v\, d\mathbf{x},$$

with F a distributed load. The symmetrical boundary condition is expressed by the normal derivative of the mid-surface deflection u as

$$-u_{,n} = \bar{\theta}_t \qquad \text{on } \Gamma.$$

Recall that Nitsche's contributions are made by *conjugate pairs*: in this case these are the rotation and the corresponding bending moment. In order to form the Nitsche contribution the direction of rotation should be consistent with the direction of corresponding bending moment (see Figure (3)).

With the choice

$$\mathbf{Bu} = -u_{,n}, \quad \boldsymbol{\tau}(\mathbf{u}) = M_{nn}(u), \quad \bar{\mathbf{B}} = \bar{\theta}_t, \quad S = \mathbb{R},$$

the Nitsche-based formulation is derived from (4) (see as well [41, 67, 53]):

$$\begin{aligned} &a(u^h, v^h) - \theta \int_\Gamma \left(-u^h_{,n}\right) M_{nn}(v^h)\, ds - \int_\Gamma M_{nn}(u^h) \left(-v^h_{,n}\right)\, ds + \gamma \int_\Gamma \left(-u^h_{,n}\right) \left(-v^h_{,n}\right)\, ds \\ &= L(v^h) - \theta \int_\Gamma \bar{\theta}_t M_{nn}(v^h)\, ds + \gamma \int_\Gamma \bar{\theta}_t \left(v^h_{,n}\right)\, ds. \end{aligned} \tag{9}$$

As previously we recover a penalty-free method by setting $\theta = -1$, $\gamma = 0$.

3.2.3. Biased frictionless contact conditions

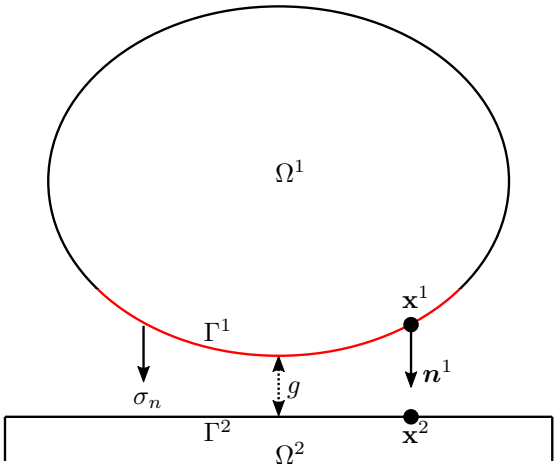

Figure 4: Contact problem setup, the contact slave surface is colored in red.

Consider a contact problem between an elastic body $\Omega := \Omega_1$ and a rigid support Ω_2 as depicted in Figure (4). Surfaces for potential contact are denoted by $\Gamma := \Gamma_1$ and Γ_2. To formulate the non-penetration condition, the normalized vector is introduced

$$\boldsymbol{n}^1 := \frac{\mathbf{x}^2 - \mathbf{x}^1}{||\mathbf{x}^2 - \mathbf{x}^1||},$$

where $\mathbf{x}^1$ and $\mathbf{x}^2$ are two mapped points on the corresponding boundary of each body Ω_1 and Ω_2, for instance $\mathbf{x}^2$ is the orthogonal projection of $\mathbf{x}^1$ on Γ_2. Then the gap function is defined as

$$g := (\mathbf{x}^2 - \mathbf{x}^1) \cdot \boldsymbol{n}^1.$$

We consider frictionless contact on Γ, which corresponds to the condition $\boldsymbol{\sigma}_{\mathbf{t}}(\mathbf{u}) = \mathbf{0}$, with $\boldsymbol{\sigma}_{\mathbf{t}}$ the tangential stress, thus the formula (5) becomes

$$a(\mathbf{u}, \mathbf{v}) - \int_{\Gamma} \sigma_n(\mathbf{u}) v_n \, ds = L(\mathbf{v}), \tag{10}$$

with the expression of $a(\cdot, \cdot)$ and $L(\cdot)$ provided in (6), and where $\sigma_n(\mathbf{u})$ (resp. v_n) is the normal component of the Cauchy stress on the boundary (resp. the normal component of the virtual displacement). The Signorini-type contact conditions (Karush-Kuhn-Tucker conditions) are expressed as (see, e.g., [23])

$$u_n - g \leq 0 \qquad \text{on } \Gamma, \tag{11a}$$

$$\sigma_n(\mathbf{u}) \leq 0 \qquad \text{on } \Gamma, \tag{11b}$$

$$\sigma_n(\mathbf{u}) \, (u_n - g) = 0 \qquad \text{on } \Gamma. \tag{11c}$$

Equation (11a) is the non-penetration condition, whereas Equation (11b) means the contact is non-adhesive, and Equation (11c) is the complementarity condition.

With the choice

$$\mathbf{B}\mathbf{u} = u_n, \quad \boldsymbol{\tau}(\mathbf{u}) = \sigma_n(\mathbf{u}), \quad \bar{\mathbf{B}} = g, \quad S = \mathbb{R}^-,$$

formulation (3) reads

$$A_\theta(\mathbf{u}^h, \mathbf{v}^h) + \frac{1}{\gamma} \int_{\Gamma} [P_1(\mathbf{u}^h) + \gamma g]_{\mathbb{R}^-} \, P_\theta(\mathbf{v}^h) \, ds = L(\mathbf{v}^h). \tag{12}$$

Remark 2. *The contact formulation is not parameter-free: for $\theta \neq -1$ the value of γ should be sufficiently large to ensure well-posedness and convergence [56, 68]. In our experience, $\gamma = E/h$ is a suitable value. For the skew-symmetric variant $\theta = -1$, the condition $\gamma > 0$ suffices to ensure the same theoretical properties, which is assessed numerically, see, e.g., [56]. Note however that the choice $\gamma = 0$ ("penalty-free") is not permitted for contact, and see for instance [52] for a first attempt at deriving a penalty-free method for Signorini contact.*

Remark 3. *When γ is extremely large, the contact detection term $[P_1(\mathbf{u}^h) + \gamma g]_{\mathbb{R}^-}$ is dominated by the displacement gap $u_n - g$, and the whole formulation behaves similarly to the penalty method. But one advantage of Nitsche's formulation is that when the current displacement gap is zero, the remaining contact normal stress term σ_n is activated to enforce contact conditions. This means that penetration in the final*

configuration, after convergence, is not necessary, and is in practice of the same order as the discretization scheme for the bulk equation.

The formulation (12) can be straightforwardly extended for biased (master-slave) contact between two elastic bodies (see, e.g., [65]), with the following modifications

$$\mathbf{Bu} = [\![u]\!]_n^{sl}, \quad \boldsymbol{\tau}(\mathbf{u}) = \sigma_n^{sl}(\mathbf{u}), \quad \bar{\mathbf{B}} = g, \quad S = \mathbb{R}^-,$$

where $[\![u]\!]_n^{sl} := (\mathbf{u}^1(\mathbf{x}^1) - \mathbf{u}^2(\mathbf{x}^2)) \cdot \boldsymbol{n}^1$ is the relative displacement written on the slave surface, and σ_n^{sl} is the contact pressure on the slave surface. Also the bilinear form $a(\cdot,\cdot)$ and the linear form $L(\cdot)$ should incorporate the virtual works of both the master and slave elastic bodies (see, e.g., [65] and references therein for details).

Remark 4. *The same methodology can be extended to other problems, involving for instance friction, dynamics and large deformations, please refer to [65] for a (non-restrictive) overview of possible extensions.*

3.3. Nitsche for interface conditions

3.3.1. Interface conditions and patch coupling

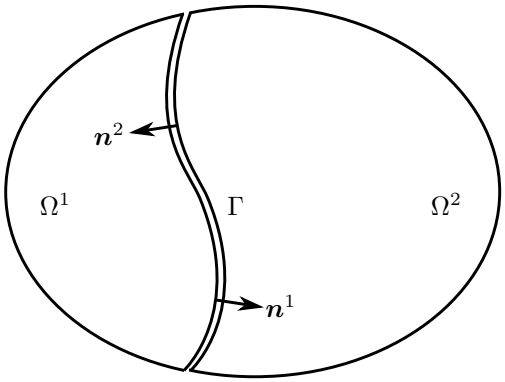

Figure 5: Problem with decomposed continuum domain. Domain Ω is decomposed into two sub-domains Ω^1 and Ω^2. The shared boundary is denoted by Γ along which the $\boldsymbol{n}^m$, $m = 1, 2$, stand for the outward unit normals.

Consider now an interface problem in which the domain Ω is decomposed into two sub-domains Ω^m (see Figure (5)), where the superscript $m = 1, 2$ is used to mark the partitioned domain and the corresponding variables. The shared boundary between Ω^1 and Ω^2 is denoted by Γ, and $\boldsymbol{n}^m$ is the unit normal along the interface Γ, pointing out of Ω^m. We still consider elasticity equations in small strains

$$-\nabla \cdot \boldsymbol{\sigma}^m = \boldsymbol{b}^m \qquad \text{in } \Omega^m,$$

with, in addition, the following interface conditions

$$\begin{aligned} \mathbf{u}^1 - \mathbf{u}^2 &= \mathbf{0} \qquad \text{on } \Gamma, \\ \boldsymbol{\sigma}^1 \boldsymbol{n}^1 + \boldsymbol{\sigma}^2 \boldsymbol{n}^2 &= \mathbf{0} \qquad \text{on } \Gamma. \end{aligned}$$

The first equation corresponds to the continuity of the displacement along the interface, while the second one is the action-reaction principle. Note that this situation corresponds both to interface problems (when, for instance, material properties are different in Ω_1 and Ω_2) and to patch coupling (where the interface between subdomains is artificial). The above equations are complemented by some essential and natural conditions on the external boundary $\partial\Omega$.

Let us define the jump and average operators along the interface Γ

$$\begin{aligned} [\![\mathbf{u}]\!] &:= \mathbf{u}^1 - \mathbf{u}^2, \\ \langle \boldsymbol{\sigma}(\mathbf{u}) \rangle &:= \frac{1}{2}(\boldsymbol{\sigma}^1(\mathbf{u})\boldsymbol{n}^1 - \boldsymbol{\sigma}^2(\mathbf{u})\boldsymbol{n}^2). \end{aligned}$$

Let us introduce also

$$\begin{aligned} a(\mathbf{u}, \mathbf{v}) &:= \sum_{m=1}^{2} \int_{\Omega^m} \boldsymbol{\sigma}^m(\mathbf{u}^m) : \boldsymbol{\epsilon}^m(\mathbf{v}^m)\, d\mathbf{x}, \\ L(\mathbf{v}) &:= \sum_{m=1}^{2} \int_{\Omega^m} \boldsymbol{b}^m \cdot \mathbf{v}^m\, d\mathbf{x} + \sum_{m=1}^{2} \int_{\Gamma_N^m} \bar{\boldsymbol{t}}^m \cdot \mathbf{v}^m\, ds. \end{aligned}$$

Green formula for elasticity equations yields

$$a(\mathbf{u}, \mathbf{v}) - \int_\Gamma (\boldsymbol{\sigma}^1(\mathbf{u})\boldsymbol{n}^1) \cdot \mathbf{v}^1\, ds - \int_\Gamma (\boldsymbol{\sigma}^2(\mathbf{u})\boldsymbol{n}^2) \cdot \mathbf{v}^2\, ds = L(\mathbf{v}).$$

Remark now that the action-reaction principle implies the following identity

$$\boldsymbol{\sigma}^1\boldsymbol{n}^1 = \frac{1}{2}\boldsymbol{\sigma}^1\boldsymbol{n}^1 + \frac{1}{2}\boldsymbol{\sigma}^1\boldsymbol{n}^1 = \frac{1}{2}\boldsymbol{\sigma}^1\boldsymbol{n}^1 - \frac{1}{2}\boldsymbol{\sigma}^2\boldsymbol{n}^2 = \langle \boldsymbol{\sigma} \rangle = -\boldsymbol{\sigma}^2\boldsymbol{n}^2.$$

It results that the appropriate Green formula in this context, which is the particular form of (1), reads

$$a(\mathbf{u}, \mathbf{v}) - \int_\Gamma \langle \boldsymbol{\sigma}(\mathbf{u}) \rangle [\![\mathbf{v}]\!]\, ds = L(\mathbf{v}). \tag{13}$$

With the choice

$$\mathbf{Bu} = [\![\mathbf{u}]\!], \quad \boldsymbol{\tau}(\mathbf{u}) = \langle \boldsymbol{\sigma}(\mathbf{u}) \rangle, \quad \bar{\mathbf{B}} = \mathbf{0}, \quad S = \mathbb{R}^d,$$

formulation (4) reads:

$$a(\mathbf{u}^h, \mathbf{v}^h) - \theta \int_\Gamma [\![\mathbf{u}]\!] \langle \boldsymbol{\sigma}(\mathbf{v}) \rangle \, ds - \int_\Gamma \langle \boldsymbol{\sigma}(\mathbf{u}) \rangle [\![\mathbf{v}]\!] \, ds + \gamma \int_\Gamma [\![\mathbf{u}]\!] [\![\mathbf{v}]\!] \, ds = L(\mathbf{v}^h). \tag{14}$$

Once again we recover a penalty-free formulation with $\theta = -1$, $\gamma = 0$. Note as well that the same formulation can be straightforwardly applied for patch coupling between plates or rods, with the appropriate changes of notations.

3.3.2. Unbiased frictionless contact

Consider that Ω^1 and Ω^2 represent two elastic bodies in frictionless contact, with no initial gap ($g = 0$). The Green formula (13) can be re-written equivalently

$$a(\mathbf{u}, \mathbf{v}) - \frac{1}{2} \int_{\Gamma^1} \sigma_n^1(\mathbf{u}^1) [\![v]\!]_n^1 \, ds - \frac{1}{2} \int_{\Gamma^2} \sigma_n^2(\mathbf{u}^2) [\![v]\!]_n^2 \, ds = L(\mathbf{v}), \tag{15}$$

with the notations $[\![v]\!]_n^1 := (\mathbf{v}^1 - \mathbf{v}^2) \cdot \boldsymbol{n}^1$ and $[\![v]\!]_n^2 := (\mathbf{v}^2 - \mathbf{v}^1) \cdot \boldsymbol{n}^2$. We now apply frictionless contact conditions on each contact surface Γ^m, $m = 1, 2$, with

$$\mathbf{Bu} = [\![u]\!]_n^m, \quad \boldsymbol{\tau}(\mathbf{u}) = \sigma_n^m(\mathbf{u}^m), \quad \bar{\mathbf{B}} = 0, \quad S = \mathbb{R}^-.$$

The following unbiased formulation for contact (see [63]) is obtained

$$A_\theta(\mathbf{u}^h, \mathbf{v}^h) + \frac{1}{2} \sum_{m=1}^{2} \int_{\Gamma^m} \frac{1}{\gamma} [P_1^m(\mathbf{u}^h) + \gamma g]_{\mathbb{R}^-} \, P_\theta^m(\mathbf{v}^h) \, ds = L(\mathbf{v}^h). \tag{16}$$

Note that this formulation does not differentiate between a master and a slave surface, and is particularly suitable for multi-body contact and self-contact (see [63, 69] for details).

4. Numerical studies

To study the performance of the proposed skew-symmetric Nitsche method, we present some numerical tests. To avoid the effects of quadrature strategies, unless otherwise specified, elements with C^{p-1} continuity are adopted for order p, and $p + 1$ Gauss quadrature points are used in this direction for each element. All

the methods are implemented by the help of the open source C++ IGA framework *Gismo* [1] [70].

4.1. Linear boundary conditions

4.1.1. Dirichlet boundary conditions patch test

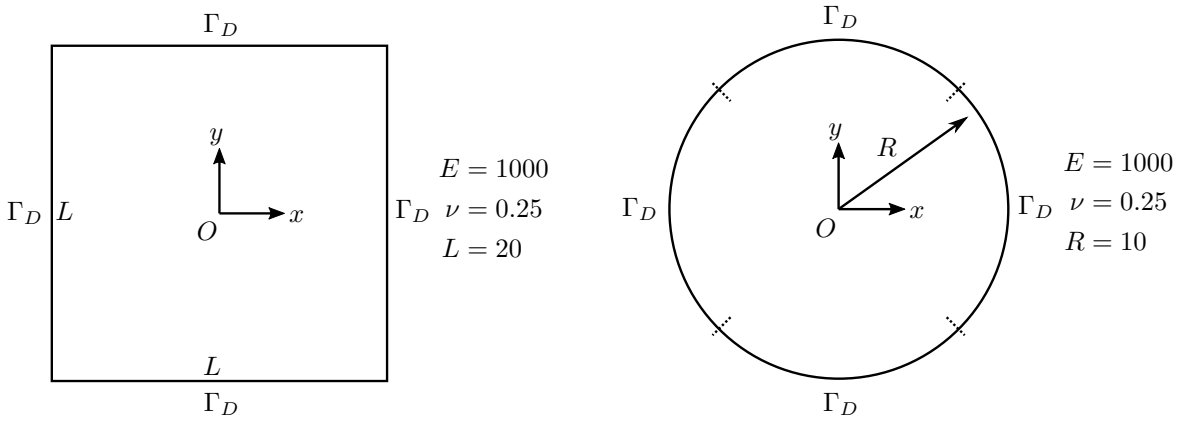

(a) Rectangular patch (b) Circular patch

Figure 6: Patch test problems.

In this section we illustrate the skew-symmetric Nitsche formulation is able to pass the rectangular patch test and has optimal convergence rate for circular shaped patch test. The B-type patch test [71] is adopted to verify the effectiveness of the introduced skew-symmetric Nitsche method: in Figure (6) we consider a linear elastic media in a square (resp. circular) domain of length $L = 20$ (resp. radius $R = 10$), with a Young modulus $E = 1000$ and a Poisson's ratio $\nu = 0.25$. The B-type patch test implies that we restrict all the boundaries according to the given displacement field, then after solving the system of equations we check the internal displacement field to inquire whether it matches the given displacement field. In order to fulfill the an equilibrium strain condition, a displacement field up to fourth order is set up as in [72]:

$$\begin{cases} u(x,y) = \frac{1}{4} + x + 3y - 2x^2 - 4xy + \frac{5}{2}y^2 - 2x^3 + x^2y - 4xy^2 - \frac{1}{3}y^3 - \frac{7}{32}x^4 - \frac{19}{24}x^3y + x^2y^2 + xy^3 - \frac{11}{96}y^4, \\ v(x,y) = 1 + \frac{1}{2}x + 2y - \frac{2}{3}x^2 + \frac{17}{5}xy + \frac{3}{2}y^2 + \frac{1}{3}x^3 + 12x^2y - xy^2 - \frac{2}{3}y^3 - \frac{11}{96}x^4 + x^3y + x^2y^2 - \frac{19}{24}xy^3 - \frac{7}{32}y^4. \end{cases}$$

For example, if the patch test of order one is performed, then the displacement field is truncated as

$$\begin{cases} u(x,y) = \frac{1}{4} + x + 3y, \\ v(x,y) = 1 + \frac{1}{2}x + 2y. \end{cases}$$

[1] https://ricamsvn.ricam.oeaw.ac.at/trac/gismo/wiki/WikiStart

The relative error of displacement u in L^2 norm are used to evaluate the performances numerically

$$\frac{\|\mathbf{u}^h - \mathbf{u}^{ref}\|_{L^2(\Omega)}}{\|\mathbf{u}^{ref}\|_{L^2(\Omega)}},$$

in which

$$\|\mathbf{u}\|_{L^2(\Omega} := \sqrt{\int_\Omega \mathbf{u}\cdot\mathbf{u}\, d\mathbf{x}}\,.$$

Table 1: The rectangular patch test is passed (Y) by the skew-symmetric Nitsche formulation.

Patch test order	1	2	3	4
IGA $p = q = 2$	Y	Y	N	N
IGA $p = q = 3$	Y	Y	Y	N
IGA $p = q = 4$	Y	Y	Y	Y

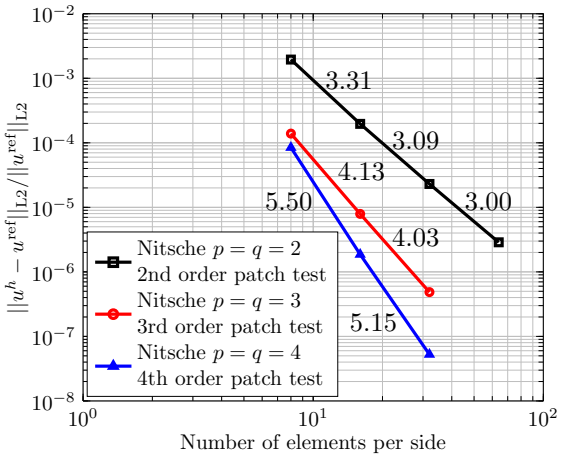

Figure 7: Optimal convergence rate is obtained for the circular patch test by the skew-symmetric Nitsche method.

The results of the rectangular patch test are given in Table 1, showing that with the Dirichlet boundary conditions being applied by the skew-symmetric Nitsche method, IGA with basis functions of a certain order is able to pass the same order patch test. The circular patch test cannot be passed exactly, because Nitsche's method imposes the boundary constraints weakly for curved boundaries. However according to Figure (7) the errors of circular patch tests become smaller as the mesh is refined, because for more refined mesh there are more elements along the boundaries to perform boundary integrations. It is observed that optimal convergence rate [73] is obtained for the circular patch test by the skew-symmetric Nitsche method, i.e. rate of $\min(p, q) + 1$ in L^2 norm.

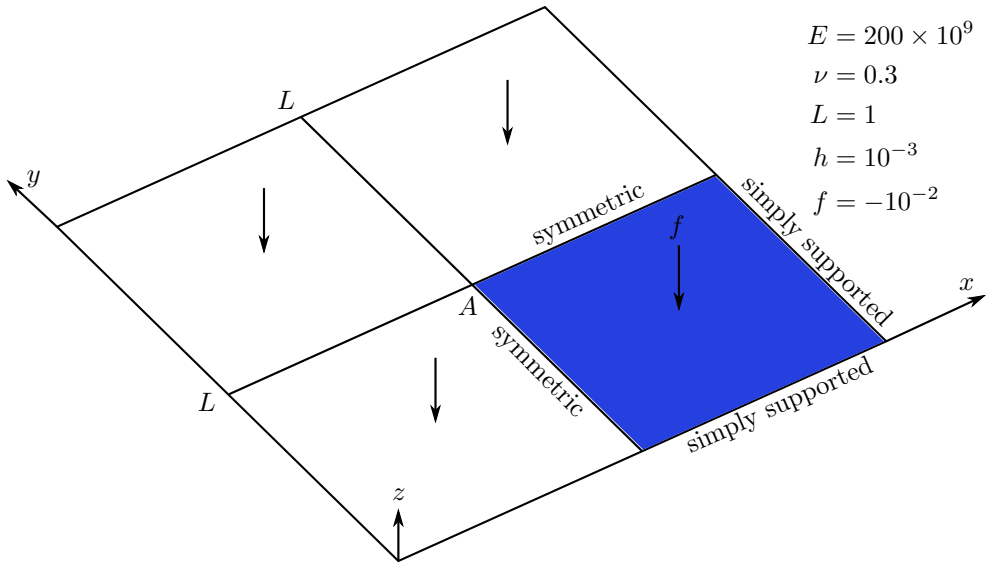

Figure 8: Square thin plate under uniform load, only 1/4 of the plate (blue area) is modeled.

4.1.2. Symmetry conditions for Kirchhoff plates

In this section we illustrate the effectiveness of the skew-symmetric Nitsche formulation to handle rotational boundary conditions for Kirchhoff plates. Figure (8) describes a simply supported thin square plate subjected to a uniform pressure. The analytical solution [74] is taken as the reference solution, which is $w_A = -2.21804 \times 10^{-6}$ [75] at point A. Due to the symmetry of this problem, only one quarter of the geometry is modeled, where two of the model boundaries are simply supported, and the other two require symmetric constraints:

$$\theta_x(x, y) = 0 \qquad \text{on } y = \frac{L}{2},$$
$$\theta_y(x, y) = 0 \qquad \text{on } x = \frac{L}{2},$$

meaning that along the boundary $y = \frac{L}{2}$ (resp. $x = \frac{L}{2}$) the rotation along x (resp. y) axis is zero. The symmetric boundary conditions can be also expressed in the local coordinate form as

$$\bar{\theta}_t = 0 \qquad \text{on } y = \frac{L}{2} \text{ and } x = \frac{L}{2},$$

in which the subscript t denotes the tangential direction of the boundary.

We firstly implement the 'second row' strategy by penalty method for comparison [14]. As illustrated in Figure (9), the idea of the 'second row' strategy consists in enforcing the displacements of the control points

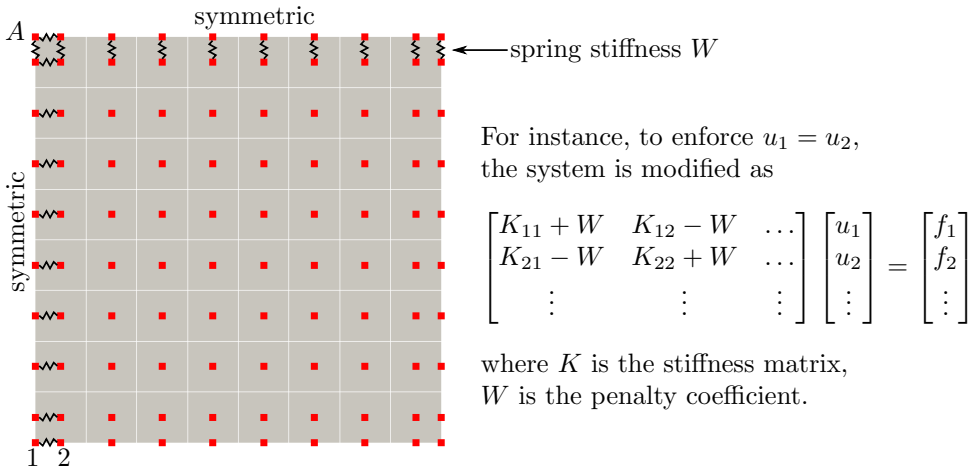

Figure 9: The 'second row' strategy with penalty method to impose the symmetry boundary conditions. The four control points near point A are penalized twice.

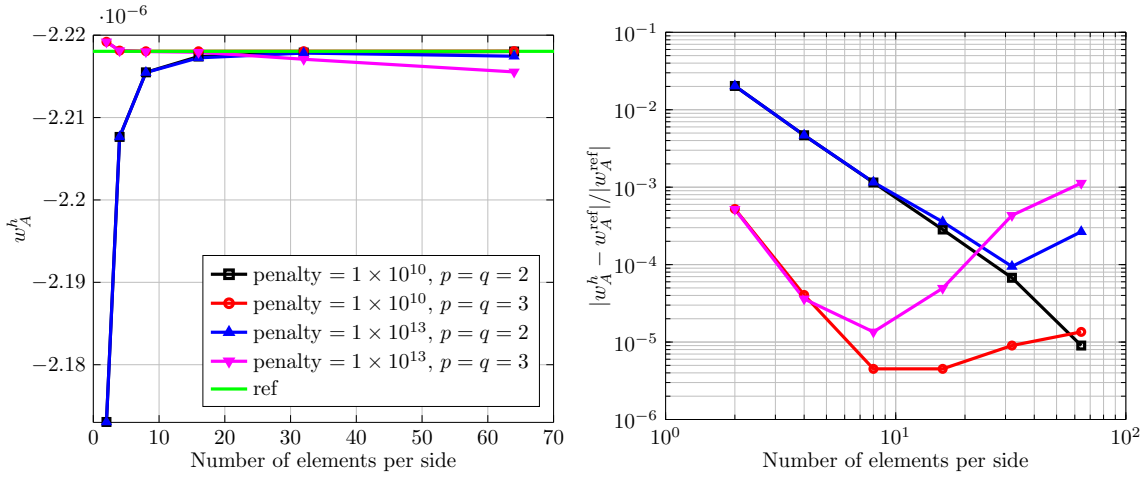

(a) Deflection w_A

(b) Relative error

Figure 10: Results for the 1/4 Kirchhoff plate. Symmetric rotational boundary conditions are imposed by the 'second row' strategy using penalty method. The results are highly sensitive to the penalty parameter.

along the symmetric boundary and the neighboring row to be equal, this is achieved by adding a penalty coefficient W in the stiffness matrix [2]. In the second row penalty method, the convergence results depend significantly on the penalty parameters, and near the Dirichlet boundary corner point A, the constraints of the four control points are penalized twice (see Figure (9)), which makes the corner deflection even more sensitive to the penalty coefficient. The results using different penalty parameters are shown in Figure (10). It is concluded that a suitable value of penalty parameter should be chosen carefully for different meshes and orders.

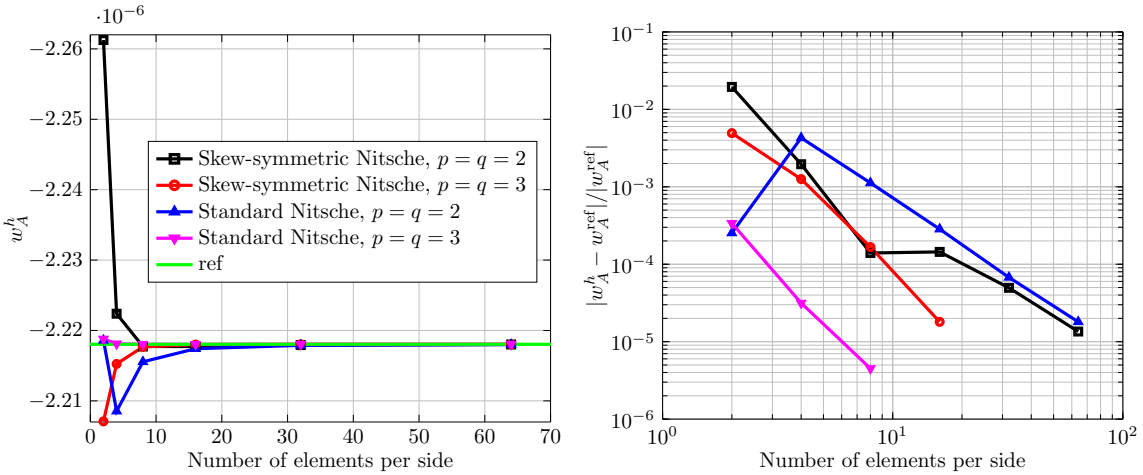

(a) Deflection w_A

(b) Relative error

Figure 11: Results for the 1/4 Kirchhoff plate. Symmetric rotational boundary conditions are imposed by the standard and skew-symmetric Nitsche methods, and the obtained results converge to the reference.

The results obtained by Nitsche's method are shown in Figure (11). The stabilization parameter for the standard Nitsche formulation is acquired by solving the generalized eigenvalue problem along the boundary [41]. Note that for $p = q = 2$ convergence of the standard and skew-symmetric Nitsche formulations are not monotonous, which is due to the deflection w_A passes through the reference solution for coarse mesh as shown in the left figure. For $p = q = 3$ this behavior disappears, and the corresponding convergence rates are slightly higher than $p = q = 2$. Finally both standard and skew-symmetric Nitsche formulations converge to the reference solution.

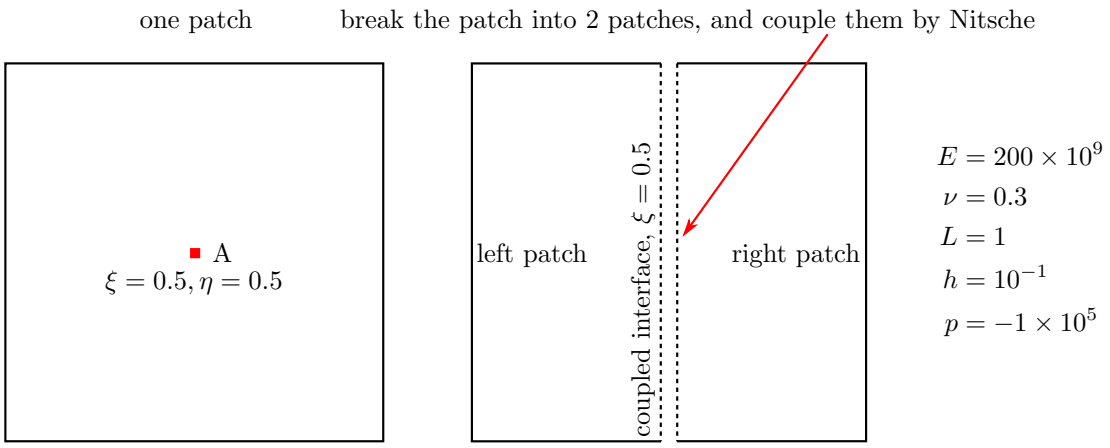

Figure 12: Plate model. On the left, one patch model is adopted as the control group. On the right, the plate is artificially broken into two conforming patches and the interface is coupled by Nitsche's method.

4.2. Linear interface conditions and patch coupling effects

4.2.1. Statics

In this section, we study whether additional effects are introduced into the accuracy, convergence performance and condition numbers when a patch coupling in statics is performed by Nitsche's method. The problem setup is shown in Figure (12), in the right figure the model is artificially broken into two identical patches. The deflection at point A at the parameter center ($\xi = 0.5, \eta = 0.5$) is denoted by w_A. The result obtained by IGA using one patch with 1,024 elements of $p = q = 5$ is $w_A = -2.52083 \times 10^{-5}$, and this is adopted as the reference value.

The convergence performance is plotted in Figure (13). By artificially breaking the patch into two patches and couple them by Nitsche's method, the obtained errors is to some degrees different from the one patch case. For higher order elements the skew-symmetric formulation performs more accurately than the standard formulation. As we refine the mesh both the standard and the skew-symmetric Nitsche formulations converge to the reference.

The deflection w along the interface ($\xi = 0.5, \eta = 0.45 - 0.55$) is shown in Figure (14) for different meshes and orders, including the solutions from the left patch and the right patch coupled by Nitsche's method. It can be seen that for this example, in which the meshes from either side of the interface are perfectly matched, the interfaces from the left patch and the right patch can be fully coupled by the standard Nitsche and the skew-symmetric Nitsce formulations, i.e. the results from the left patch and the right patch are identical. For coarse mesh of 4×4 elements, there are visible errors for Nitsche's methods, but their results

[2]http://www.colorado.edu/engineering/CAS/courses.d/IFEM.d/IFEM.Ch09.d/IFEM.Ch09.pdf

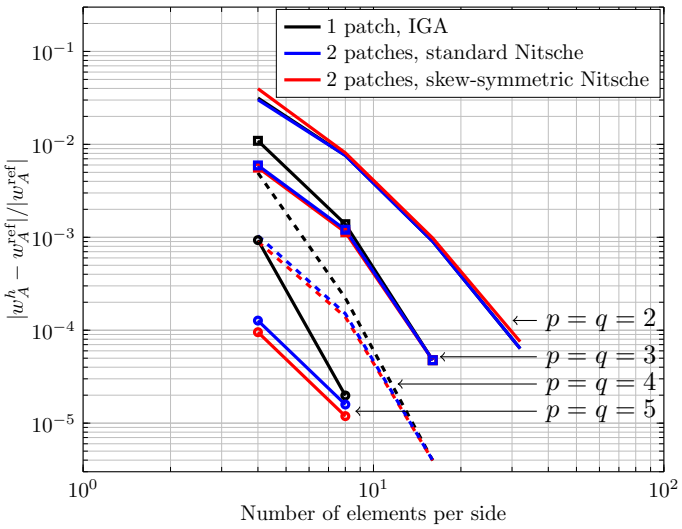

Figure 13: Relative errors of w_A. Both the standard and the skew-symmetric Nitsche formulations converge to the reference.

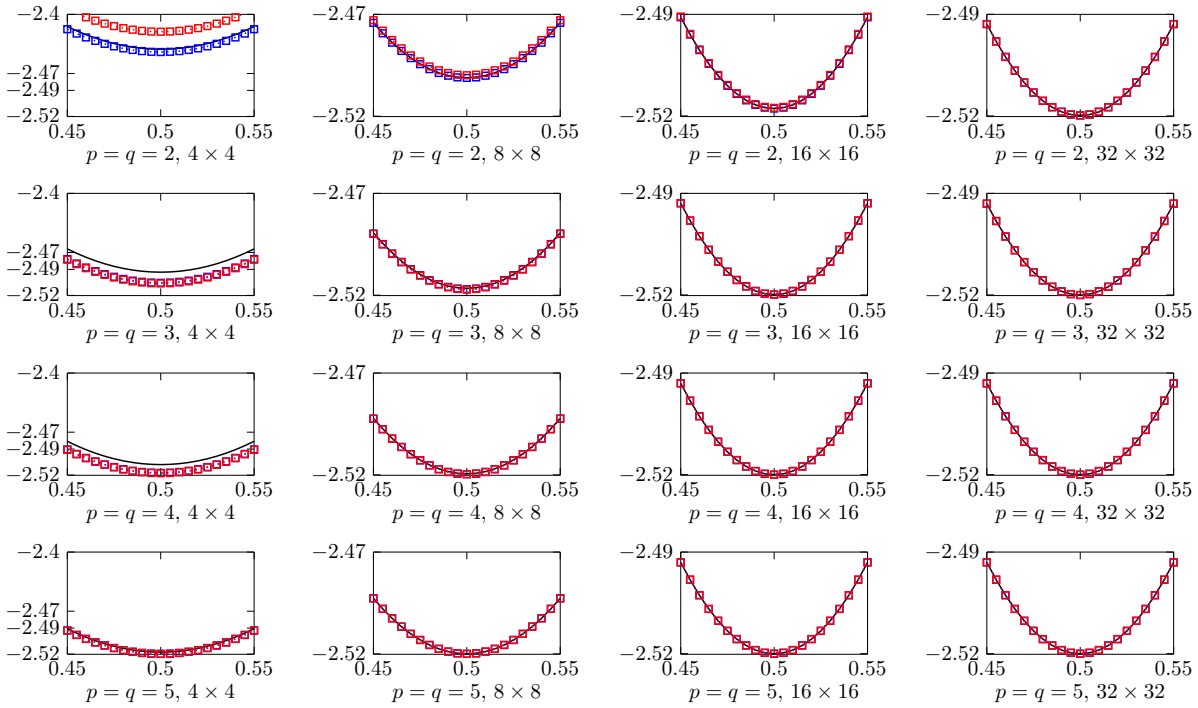

Figure 14: w along interface ($\xi = 0.5, \eta = 0.45 - 0.55$). By coupling the interface by Nitsche's method, the results from the left patch and the right patch are identical, and their results tend to the reference as the mesh is refined.
Horizontal axis: η. Vertical axis: $w^h \times 10^{-5}$. — 1 patch IGA.
2 patches standard Nitsche, the left patch. - - - 2 patches standard Nitsche, the right patch.
2 patches skew-symmetric Nitsche, the left patch. - - - 2 patches skew-symmetric Nitsche, the right patch.

tend to the reference as the mesh is h-refined (from left to right), p-refined (from top to bottom) or k-refined (diagonal, from the upper left corner to the lower right corner).

Table 2: Condition numbers ($\times 10^{10}$) of the obtained stiffness matrix. The standard Nitsche formulation increases the condition number significantly.

Method	Number of elements per side	$p = q = 2$	$p = q = 3$	$p = q = 4$	$p = q = 5$
IGA	4	0.926	0.884	0.858	0.850
	8	0.958	0.979	1.103	1.238
	16	0.959	1.002	1.161	1.347
standard	4	8.942	15.033	21.711	28.011
Nitsche	8	11.963	18.104	23.693	29.033
	16	13.301	21.680	29.204	35.938
skew-symmetric	4	1.919	1.340	1.285	1.256
Nitsche	8	2.118	2.055	2.039	2.035
	16	2.174	2.487	2.723	2.887

The condition numbers of the obtained stiffness matrix are given in Table (2). From a general point of view, h-refinement of the mesh, which means that using more control points, increases the corresponding condition number. It is noticed that the condition number obtained from Nitsche's coupling is larger than one patch IGA, this is inferred to be related to the coupling effects. Specifically, the skew-symmetric Nitsche formulation slightly increases the condition number compared to IGA because there are more control points along the coupled interface. The stabilization parameter for the standard Nitsche formulation and it is usually a large value, which is acquired by solving the generalized eigenvalue problem along the boundary [41, 43]. The standard Nitsche formulation increases the condition number significantly, which is inferred to be attributed to the adopted stabilization parameter.

4.2.2. Modal analysis

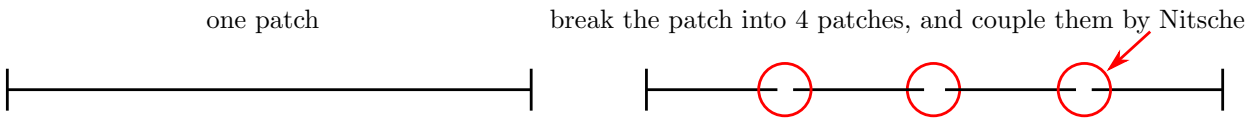

Figure 15: Rod model. On the left, one patch rod model is adopted as the control group. On the right, the rod is artificially broken into four patches and the additional three interfaces are coupled by Nitsche's method.

To study whether additional effects are introduced in modal analysis by Nitsche's coupling, the longitudinal vibration of a rod [58] is considered (Figure (15)). In the right figure the rod model is broken into four

identical patches and they are coupled by Nitsche's method. The governing equations of this problem are

$$u_{,xx} + \omega^2 u = 0,$$

$$u(0) = u(1) = 0,$$

where $x \in [0, 1]$ denotes the rod's length, and the exact natural frequencies are

$$\omega_n = n\pi, \quad n = 1, 2, \ldots.$$

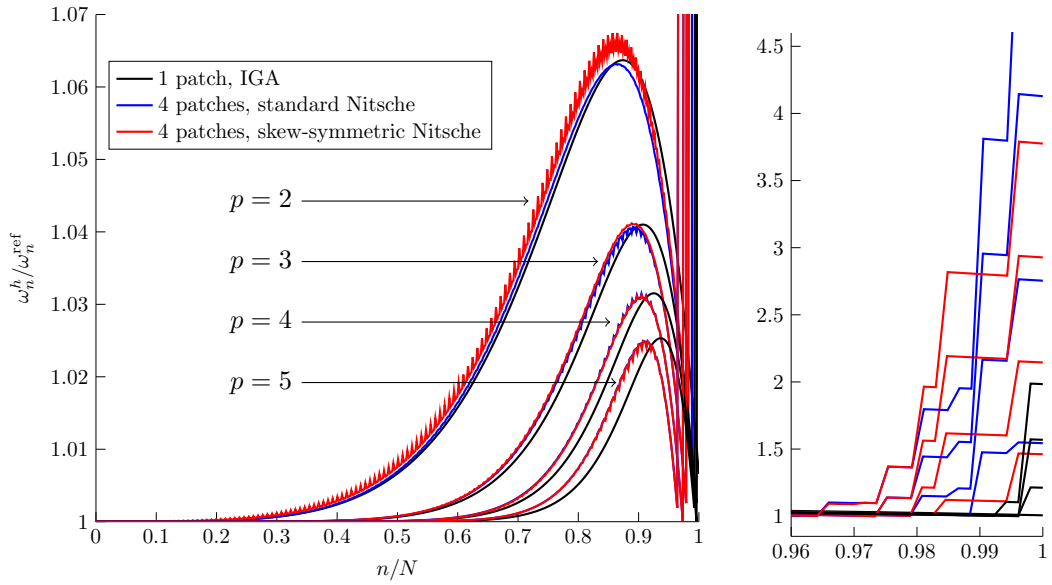

Figure 16: Normalized discrete spectra. As shown in the right figure, the sudden jump of the frequencies identify the 'outliers'. More details are shown in Figure (17).

The discrete spectra is independent of the total number of DoFs N if it is normalized by N. Nevertheless to get a relatively smooth spectra the mesh should be very well refined, here more than 500 control points are used. The normalized discrete spectra is given in Figure (16), showing that Nitsche's coupled model is almost as accurate as conforming IGA for lower frequencies, specifically $n < 0.2$ for $p = 2$ and $n < 0.5$ for higher orders. For higher order frequencies, the skew-symmetric Nitsche leads to oscillations when $p = 2$, and both standard and skew-symmetric Nitsche solutions are oscillatory when $p = 3, 4, 5$.

At the very end of the spectra, the sudden jump of the frequencies are known as the 'outliers' [58, 59, 60], as shown in the enlarged figure on the right side of Figure (16). These 'outlier' frequencies are drawn in Figure (17), and the number of outliers is also counted. The 'outlier' frequencies are captured near $n = 1$ by the

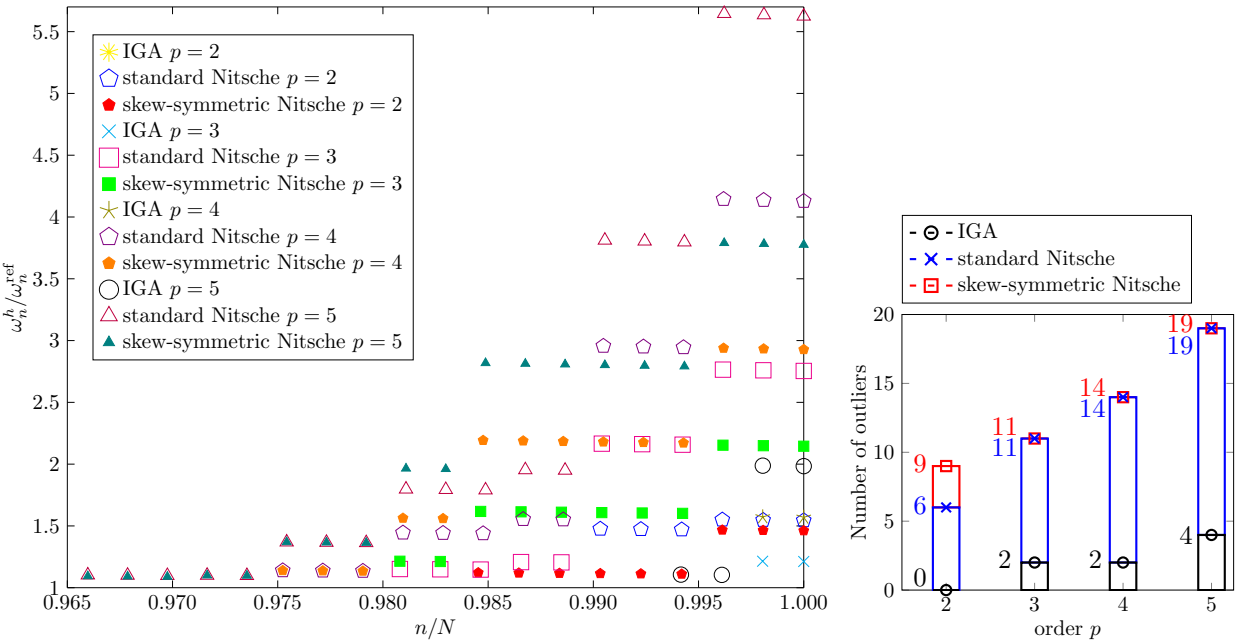

Figure 17: Normalized outlier frequencies. The model coupled by Nitsche's leads to a larger number of 'outliers'. The corresponding outlier eigenmodes of $p = 2$ are plotted in Figure (18) for the standard Nitsche formulation and in Figure (19) for the skew-symmetric Nitsche formulation.

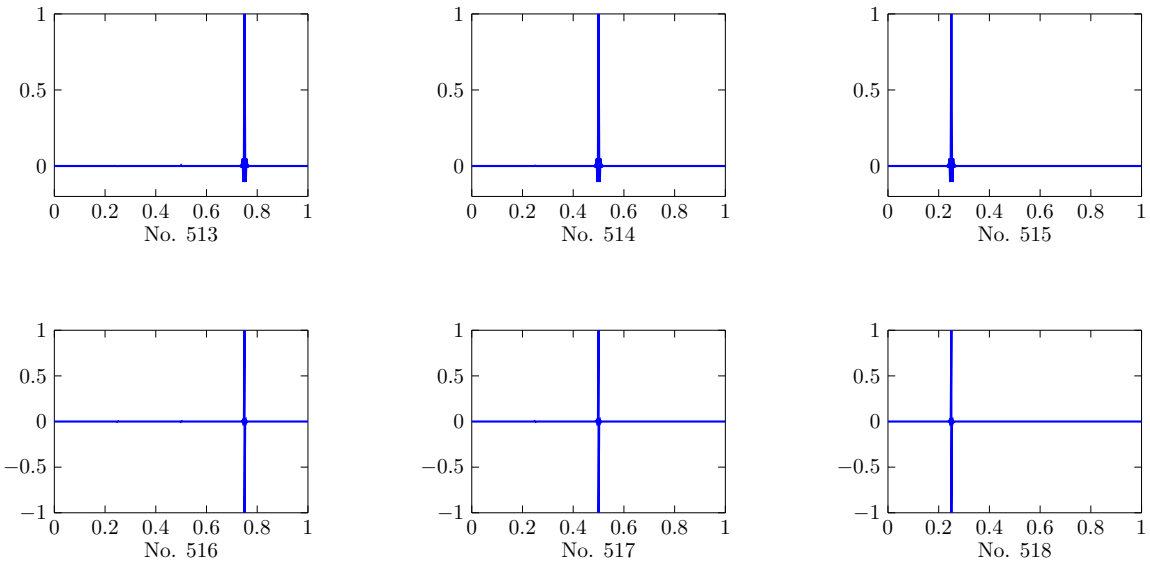

Figure 18: 'Outlier' (last 6 out of 518) eigenmodes obtained by the standard Nitsche formulation with $p = 2$. The longitudinal deformations are plotted along the vertical axis. The eigenmodes that correspond to the 'outliers' are highly localized at the coupled interfaces.

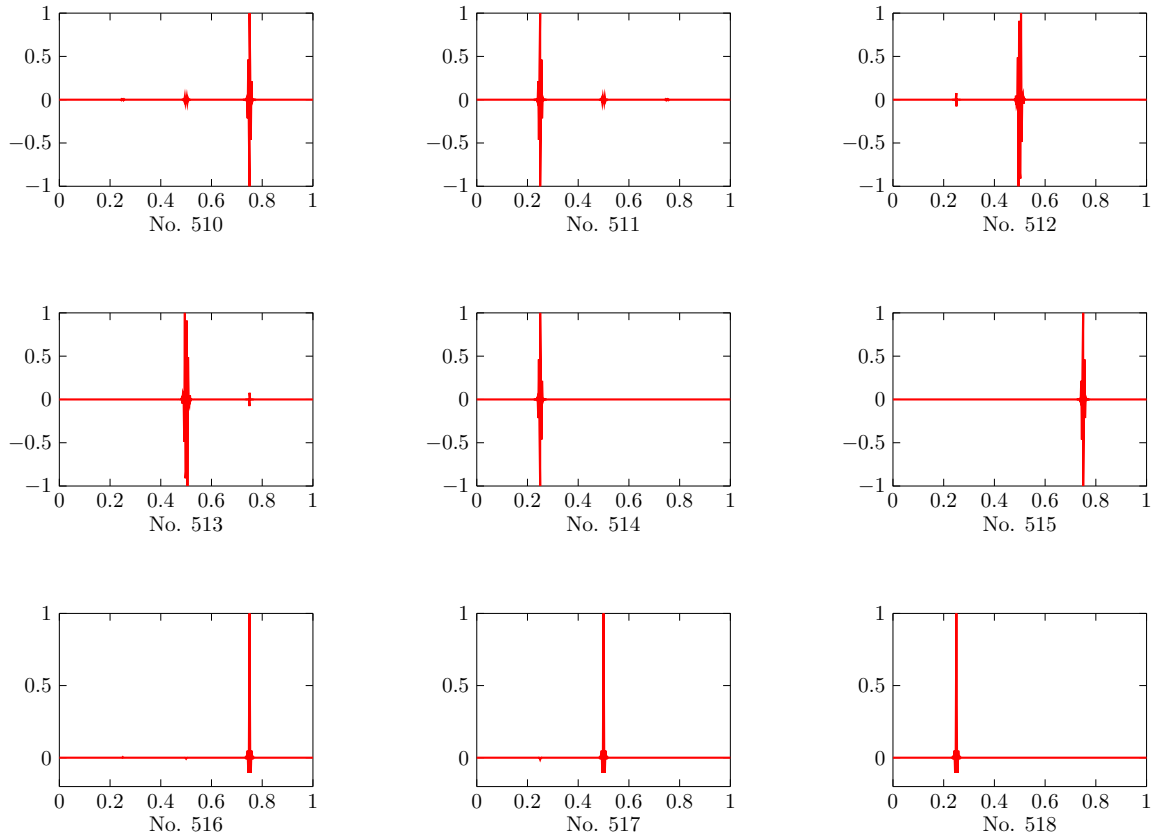

Figure 19: 'Outlier' (last 9 out of 518) eigenmodes obtained by the skew-symmetric Nitsche formulation with $p = 2$. The longitudinal deformations are plotted along the vertical axis. The eigenmodes that correspond to the 'outliers' are highly localized at the coupled interfaces.

conforming IGA, and the model coupled by Nitsche's formulation leads to a larger number of 'outliers'. The corresponding outlier eigenmodes of $p = 2$ are plotted in Figure (18) for the standard Nitsche formulation and in Figure (19) for the skew-symmetric Nitsche formulation. To achieve a better demonstration of the eigenmodes, we plot the longitudinal deformation along the vertical axis. The number of 'outliers' obtained by the skew-symmetric Nitsche formulation is three more than the standard Nitsche when $p = 2$, because there exist 3 pairs of symmetrical eigenmodes, i.e. no.510 and no.511, no.512 and no.513, no.514 and no.515. These results imply that the action that coupling the artificially broken interfaces by Nitsche's method increases the number of 'outliers', and the eigenmodes correspond to the 'outliers' are highly localized at these coupled interfaces.

4.3. Contact

4.3.1. Contact between two blocks

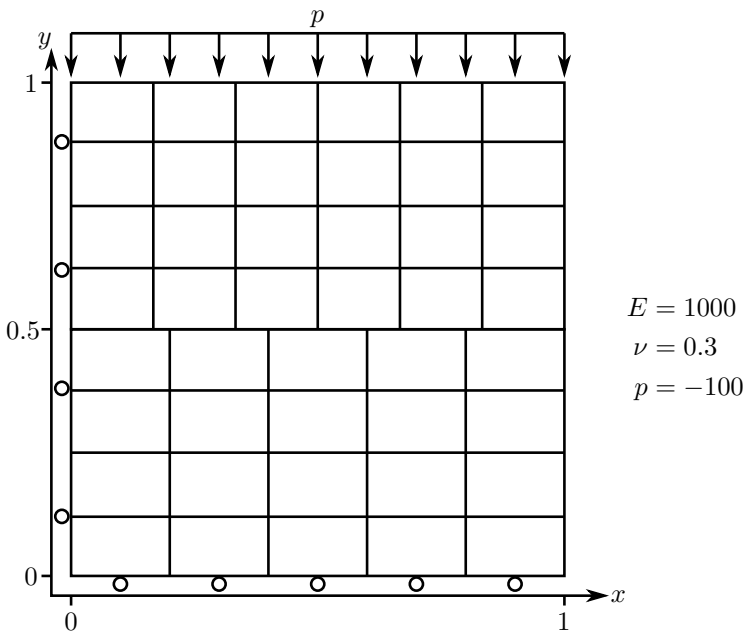

Figure 20: Two blocks with non-matching meshes. The upper block is subjected to uniformed pressure p. Both blocks have the same material property. The problem setup is not symmetric due to the boundary conditions along the left sides of the two blocks.

The objective of this section is to test whether the proposed formulation can properly impose the contact conditions through matching and non-matching elements, and preliminarily investigate the robustness of the skew-symmetric Nitsche formulation with respect to the contact interface element length ratio, the number of quadrature points and the value of γ. The classical contact patch test proposed by Taylor [76] is used to examine the contact algorithm and investigate whether it transfer the constant contact pressure through

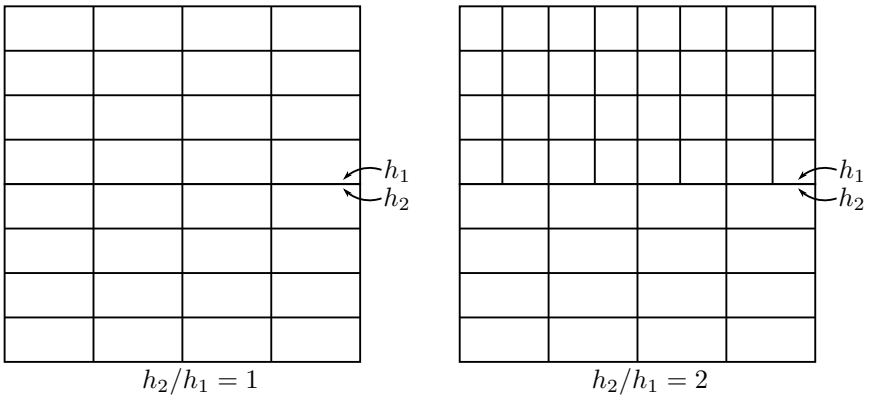

Figure 21: Two blocks with matching meshes. The boundary conditions and materials are the same as in Figure (20). We refine the upper block to get various interface element length ratios $h_2/h_1 = 1, 2, 4, 8, 16$.

the contact surface even for non-matching meshes [77]. In order to enforce a uniform pressure on the top surface more easily, we adopt a modified patch test [78, 79] as shown in Figure (20). The resulting test setup is similar as in [80]. Because of the boundary conditions along the left sides of the two blocks, this problem setup is not symmetric. The reference solution of the (plane stress) problem is that

$$\begin{aligned} u_y(x, y) &= -0.1y, \\ \sigma_y(x, y) &= -100. \end{aligned} \tag{17}$$

Table 3: The number of Gauss quadrature points (#GP) per slave element and the corresponding number of Newton-Raphson iterations (#NR) to achieve convergence (tolerance threshold for the residual 1×10^{-4}). (p, q) are basis function orders. h_2/h_1 denotes element length ratio. $\gamma = E$. The 'FAIL' denotes that the convergence is not achieved after trying from 1 to 10 quadrature points in 100 Newton-Raphson iterations.

$p = q = 2$	h_2/h_1	1	2	4	8	16
standard Nitsche	#GP	2	2	2	2	2
	#NR	3	4	4	4	3
skew-symmetric Nitsche	#GP	2	2	2	2	2
	#NR	3	4	4	4	3
$p = q = 3$	h_2/h_1	1	2	4	8	16
standard Nitsche	#GP	5	5	-	-	-
	#NR	35	27	FAIL	FAIL	FAIL
skew-symmetric Nitsche	#GP	5	5	5	5	-
	#NR	34	26	25	26	FAIL
$p = q = 4$	h_2/h_1	1	2	4	8	16
standard Nitsche	#GP	3	3	3	3	3
	#NR	3	6	8	6	5
skew-symmetric Nitsche	#GP	3	3	3	3	3
	#NR	3	6	8	7	6

This problem is calculated by the biased Nitsche contact formulation, however [63] shows that for both

biased and unbiased versions the accuracy is comparable. Firstly we investigate the influence of the number of quadrature points with respect to various element size ratios and basis function orders. From the matching meshes as illustrated in Figure (21), we refine the upper block in order to obtain various interface element length ratios, specifically $h_2/h_1 = 1, 2, 4, 8, 16$. Here we fix $\gamma = E$ and adopt a criteria of the residual tolerance 1×10^{-4}. We try to find a unified number of Gauss quadrature points for certain basis function orders (p, q) such that the problem converges for as many ratio cases as possible. The results are given in Table (3), where the 'FAIL' denotes that the convergence is not achieved after trying from 1 to 10 quadrature points per slave boundary element in 100 Newton-Raphson iterations. It is deduced that for $p = q = 3$ the problem is hard to converge, there is no theoretical explanation for the failure yet, but to our computational experience, in these cases the top block moves back and forth drastically from current iteration to the next iteration. While for $p = q = 2$ and $p = q = 4$ it is feasible to use 2 and 3 quadrature points per slave boundary element respectively.

Table 4: Newton-Raphson iterations and the max vertical displacement for various γ and various numbers of quadrature points (#GP). $p = q = 2$. $h_2/h_1 = 1.2$. $\max(u)^{\text{ref}} = -0.1$. The 'FAIL' means that the convergence is not achieved within 100 Newton-Raphson iterations. The skew-symmetric Nitsche formulation behaves robust with respect to the value of γ. Using more quadrature points could achieve better accuracy.

γ	standard Nitsche						skew-symmetric Nitsche					
	#GP=2		#GP=3		#GP=5		#GP=2		#GP=3		#GP=5	
1/100	25	-0.10007	23	-0.10006	FAIL	-	21	-0.10008	18	-0.10006	29	-0.1
1/10	26	-0.10007	23	-0.10006	FAIL	-	21	-0.10008	18	-0.10006	26	-0.1
1	24	-0.10007	23	-0.10006	FAIL	-	21	-0.10008	18	-0.10006	13	-0.1
10	23	-0.10007	18	-0.10006	FAIL	-	15	-0.10008	18	-0.10006	13	-0.1
100	17	-0.10007	18	-0.10006	13	-0.1	15	-0.10008	19	-0.10006	13	-0.1
E	17	-0.10007	18	-0.10006	13	-0.1	15	-0.10008	19	-0.10006	13	-0.1
10000	19	-0.10007	19	-0.10006	14	-0.1	16	-0.10008	20	-0.10006	14	-0.1

The following test is performed by non-matching meshes with $p = q = 2$. The meshes are given in Figure (20) and the interface element length ratio is $h_2/h_1 = 1.2$. The performances of standard and skew-symmetric Nitsche formulations using various values of γ are tested. The number of Newton-Raphson iterations and the max vertical displacement for various γ are given in Figure (4). According to Table (3), we test 2, 3 and 5 quadrature points respectively per slave element. The convergence criteria of the residual tolerance is 1×10^{-4}. The results are given in Table (4). The 'FAIL' means that the convergence is not achieved within 100 Newton-Raphson iterations. Using the standard Nitsche formulation with $E = 1000$, convergence is achieved for all $\gamma = E/10, E, 10E$. The skew-symmetric Nitsche formulation behaves robust with respect to the value of γ, and convergence is achieved for all the cases. Even for small values such as $\gamma = 1/10$ and $\gamma = 1/100$, the convergence is achieved by the skew-symmetric Nitsche formulation, by taking

more Newton-Raphson iterations. It is noticed that when using 2 quadrature points or 3 quadrature points per slave boundary element, the max vertical displacement does not match the reference $\max(u)^{\text{ref}} = -0.1$. It is inferred that using more quadrature points (e.g. #GP=5) could achieve better accuracy. However for #GP=5 the price to pay is that the nonlinear system behaves more difficult to converge for the standard Nitsche formulation, as it fails for cases when γ is not large enough.

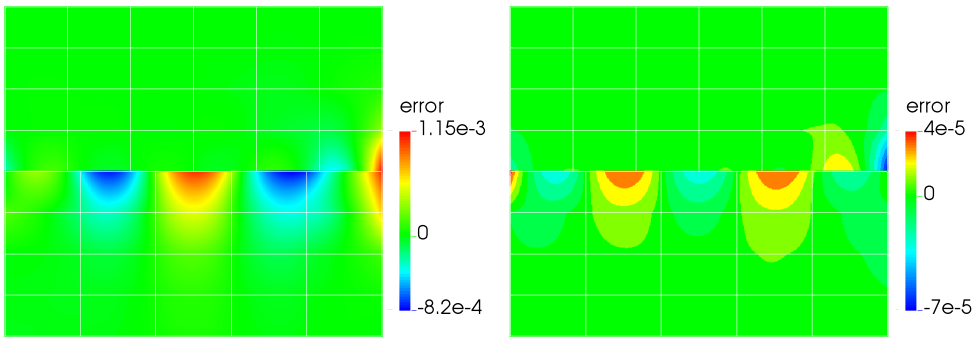

(a) 5 quadrature points (b) 15 quadrature points

Figure 22: Relative errors in stress σ_y obtained by the skew-symmetric Nitsche method, plotted on the deformed geometry. $p = q = 2$. $\gamma = E$. $\sigma_y^{\text{ref}} = -100$. For the left figure, the relative errors range from -0.082% to 0.115%. For the right figure, the relative errors range from -0.007% to 0.004%. Better accuracy can be achieved using more quadrature points per slave boundary element.

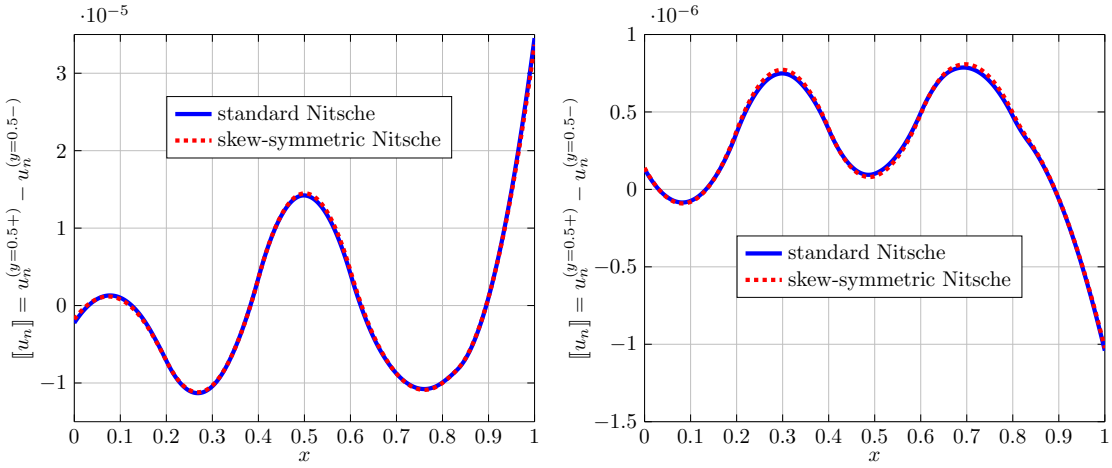

(a) 5 quadrature points (b) 15 quadrature points

Figure 23: Vertical displacement jumps $[\![u_n]\!]$ between the contact interface $y = 0.5$. $p = q = 2$. $\gamma = E$. Positive values mean there are gaps, and negative values mean there are overlaps. Better accuracy can be achieved using more quadrature points per slave boundary element.

The relative errors in stress σ_y, the vertical displacement jumps $[\![u_n]\!]$ and the contact stress $\sigma_n^1(\mathbf{u})$ are given in Figure (22), Figure (23) and Figure (24) respectively. Here we fix $\gamma = E$, use 5 quadrature points

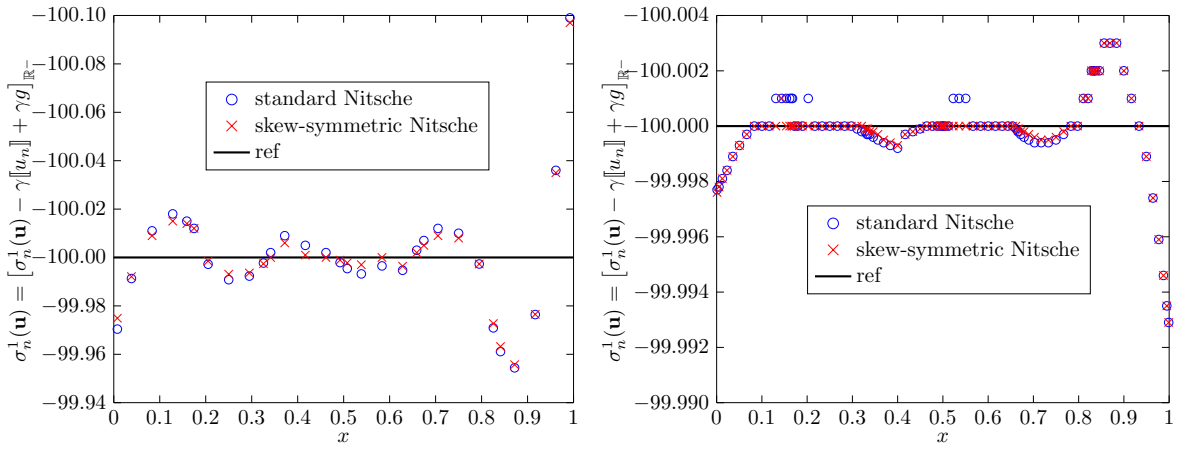

(a) 5 quadrature points

(b) 15 quadrature points

Figure 24: Contact stress $\sigma_n^1(\mathbf{u})$ at quadrature points along the contact elements. $p = q = 2$. $\gamma = E$. Better accuracy can be achieved using more quadrature points per slave boundary element.

per slave boundary element, and set the convergence criteria of the residual tolerance as 1×10^{-4}. In order to get solutions with lower errors, we also use 15 quadrature points per slave boundary element, and set the convergence criteria of the residual tolerance as 1×10^{-10}. From these results it is shown that lower errors can be achieved by using more quadrature points per slave boundary element along with smaller convergence criteria.

4.3.2. Hertz contact

In this section we show that the proposed skew-symmetric Nitsche contact formulation is robust w.r.t. the choice of Nitsche's parameter γ, and it is able to predict the contact pressure distribution versus contact width to some degrees of accuracy. Here we study a contact problem as shown in Figure (25) with analytical solution provided by Hertz [81]. The Hertz contact assumes an elastic frictionless contact without adhesive forces between two cylinders with the same height, radii R_1, R_2 and elasticity moduli E_1, E_2. To simplify, the master body is fixed, its material is set to be rigid, and its contact surface is flat. In this special case, since $E_2 \to \infty$ and $R_2 \to \infty$, the contact modulus and equivalent radius become

$$E^* = \frac{E_1 E_2}{E_2(1-\nu_1^2) + E_1(1-\nu_2^2)} = \frac{E_1}{1-\nu_1^2}, \quad R^* = \frac{R_1 R_2}{R_1 + R_2} = R_1.$$

With the total exerted normal force being $F_n = g \times \pi r^2$, the maximum pressure and the half contact width are given by

$$p_{\max} = \sqrt{\frac{F_n E^*}{\pi R^*}} = 2.2918 \times 10^6, \quad a = \sqrt{\frac{4 F_n R^*}{\pi E^*}} = 0.0454,$$

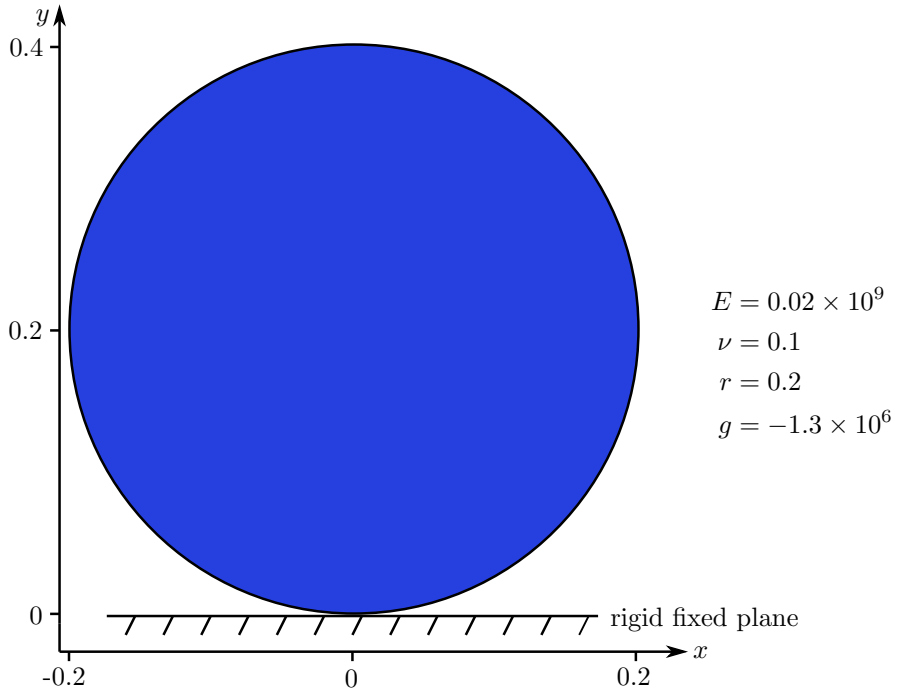

Figure 25: Hertz contact example, the contact between a linear elastic disc under a vertical gravity force and a rigid fixed plane.

and the pressure distribution is

$$p(x) = p_{\max}\sqrt{1 - \left(\frac{x}{a}\right)^2}, \quad x \in [-a, a].$$

To prevent rigid body motion along the horizontal direction, we fix the horizontal displacement at four control points along axis of $x = 0$, in parameter space they locate near the positions $(\xi = 0.5, \eta = 0)$ and $(\xi = 0.5, \eta = 1)$. The geometry is modeled using NURBS basis functions of order $p = q = 2$, and we only h-refine the elements hereafter. To achieve a balance between accuracy of results and assurance of convergence, we adopt 5 quadrature points per contact boundary element. The update norm 1×10^{-10} is employed as the tolerance threshold to control the Newton-Raphson iterations.

To begin with we draw the results for one case in Figure (26) as an illustration, with 16×16 elements and $\gamma = 100E$. The von Mises stress field is plotted using 500×500 sample points that uniformly located at the parameter space. The contour plot shows that the rigid fixed plane has successfully prevented the disc from dropping down, and the contact surface of the elastic disc adjusts itself to match the rigid fixed plane, resulting in a straight contact surface. Notice that at the four corners of the patch, the Jacobian matrix

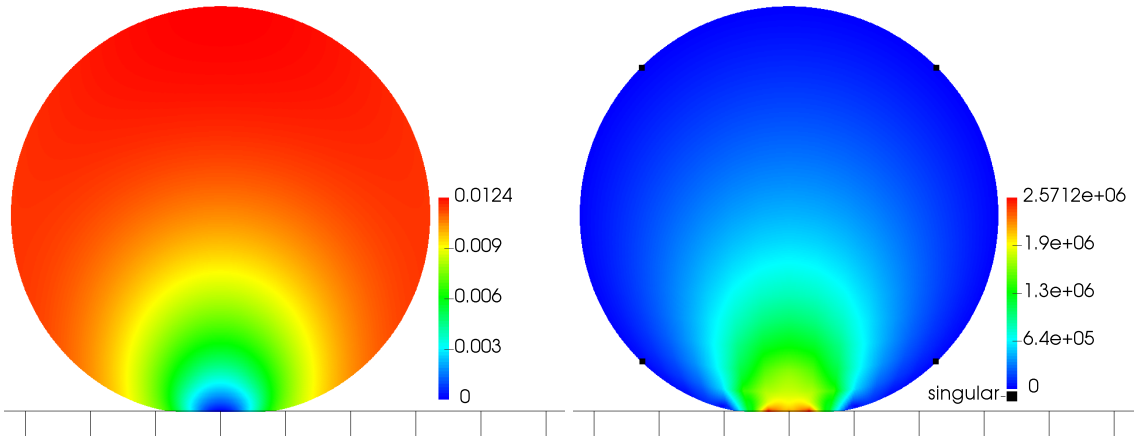

(a) displacement magnitude (b) von Mises stress

Figure 26: Contour plot of displacement magnitude field and von Mises stress field obtained by the skew-symmetric Nitsche method using 16×16 elements and $\gamma = 100E$. The rigid fixed plane has successfully prevented the disc from dropping down, and the contact surface of the elastic disc adjust itself to match the rigid fixed plane, resulting in a straight contact surface.

Table 5: Results for Hertz contact. Convergence is not achieved for the standard Nitsche method when $\gamma = E/100$ is employed. The skew-symmetric method is robust to the choice of γ.

Nitsche's type	γ	mesh	max pressure $p_{\max}^{\text{ref}} = 2.2918 \times 10^6$	relative error %	half contact width $a^{\text{ref}} = 0.0454$	relative error %	Newton-Raphson residual norm
standard	$100E$	8×8	2.8737×10^6	25.39	0.0391	-13.88	9.91×10^{-9}
		16×16	2.3416×10^6	2.17	0.0456	0.42	3.08×10^{-7}
		64×64	2.3976×10^6	4.62	0.0460	1.27	1.86×10^{-6}
standard	E	8×8	2.2349×10^6	-2.48	0.0502	10.50	2.63×10^{-6}
		16×16	2.3525×10^6	2.65	0.0509	12.17	1.81×10^{-5}
		64×64	2.3832×10^6	3.99	0.0460	1.27	1.04×10^{-4}
skew-symmetric	$100E$	8×8	2.8334×10^6	23.63	0.0391	-13.88	6.37×10^{-9}
		16×16	2.3126×10^6	0.91	0.0456	0.42	1.51×10^{-7}
		64×64	2.3564×10^6	2.82	0.0460	1.27	2.45×10^{-6}
skew-symmetric	E	8×8	2.3588×10^6	2.92	0.0502	10.50	2.58×10^{-6}
		16×16	2.3312×10^6	1.72	0.0509	12.17	1.11×10^{-5}
		64×64	2.3417×10^6	2.18	0.0460	1.27	1.12×10^{-4}
skew-symmetric	$\frac{E}{100}$	8×8	2.1940×10^6	-4.27	0.0607	33.63	2.79×10^{-4}
		16×16	2.3529×10^6	2.67	0.0509	12.17	1.90×10^{-3}
		64×64	2.3362×10^6	1.94	0.0460	1.27	1.38×10^{-2}

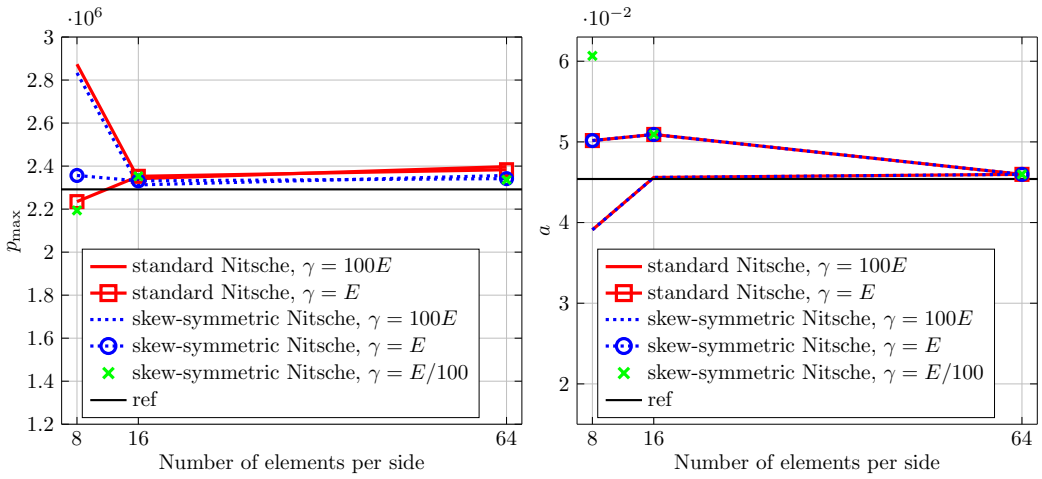

(a) max pressure $p_{\max}$ (b) half contact width a

Figure 27: Convergence of Hertz contact example. The results converge to the analytical solution as the mesh is refined, with the relative errors of max pressure ranging from 1.94% to 4.62% and half contact width being 1.27%.

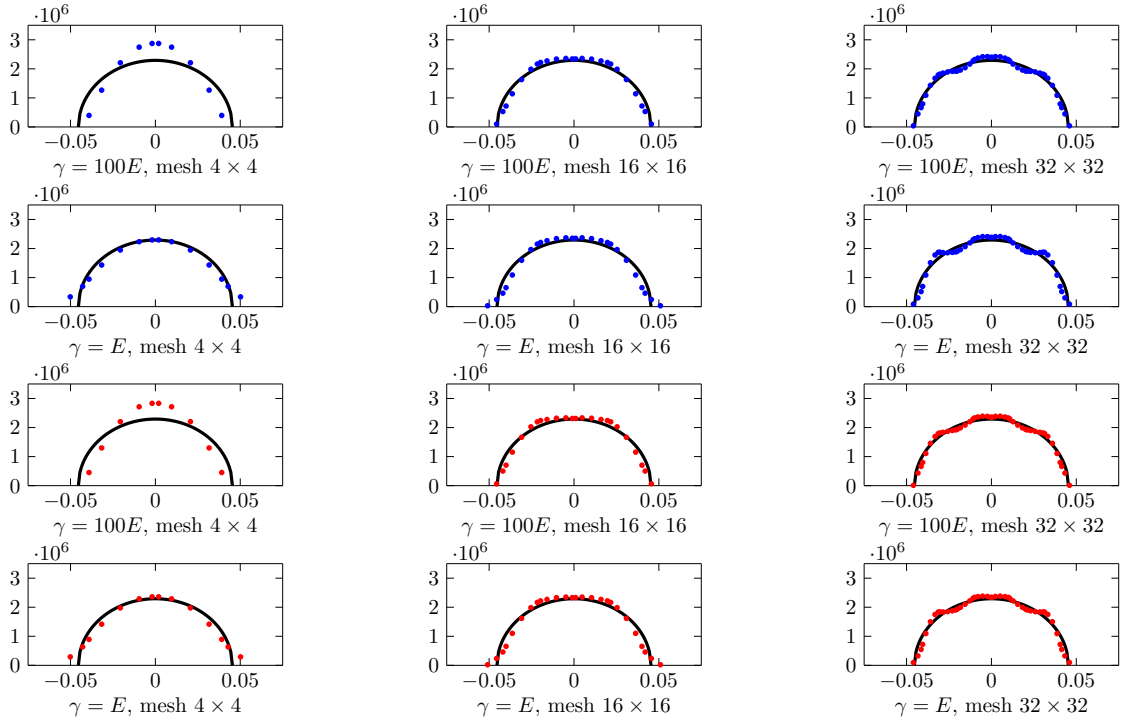

Figure 28: Pressure distribution for Hertz contact. Horizontal axis: contact surface $y = 0$. Vertical axis: contact pressure p.
— analytical solution, • the standard Nitsche method, • the skew-symmetric Nitsche method.
The contact stresses shown in blue and red dots are calculated at quadrature points. The Nitsche formulations can properly predict the pressure distribution with respect to the contact width as the mesh is refined.

is nearly non-inversible, which leads to four areas with abnormal errors along the boundary. The results of max pressure and half contact width using different meshes and values of γ are given in Table (5). The results for standard Nitsche's method with $\gamma = E/100$ is not shown because convergence is not achieved. The skew-symmetric version of the method is very robust to the choice of γ: from $100E$ to $E/100$, i.e. four orders of magnitude. Focusing on the Newton-Raphson residual norm, it is concluded that as the mesh is refined, or smaller value of γ is used such as $\gamma = E/100$, the converged residual norm decreases gradually, while the accuracy of the results of max pressure and half contact width remains acceptable. This explains the reason that in this example we use the update norm as the criteria to control the Newton-Raphson iterations instead of the residual norm. As shown in Figure (27), the results converge to the analytical solution as the mesh is refined, with the relative errors of max pressure ranging from 1.94% to 4.62% and half contact width being 1.27%. Note that the relative error is not becoming smaller because the Nitsche formulation is performed at quadrature points, meaning that the reaction force is applying to these quadrature points that are actually in contact with the rigid support, and there is no reaction force if the quadrature point is not in contact, therefore the converged results and hence the errors depend on the distribution of the quadrature points. Finally the pressure distribution with respect to the contact width is plotted comparing with the analytical solution in Figure (28), according to the fact that the stress on the contact surface reaches balance with the contact pressure. The contact stresses shown in blue and red dots are calculated at quadrature points. The Nitsche's method can properly predict the pressure distribution with respect to the contact width as the mesh is refined.

5. Conclusions

We presented a systematic way to derive a Nitsche formulation for different kind of boundary and interface conditions, and studied this technique in the context of isogeometric analysis (IGA) discretization. We recover different variants of Nitsche's method, for different values of the *Nitsche parameter* θ, and then focused on the skew-symmetric variant, namely $\theta = -1$. This variant is appealing because it does not need a stabilization term for linear boundary/interface conditions, and is robust w.r.t. the stabilization parameter for non-linear boundary/interface conditions. Several numerical studies were performed to illustrate the behavior of Nitsche's method, especially the skew-symmetric variant. From the numerical results we can state the observations below:

• The skew-symmetric formulation is effective to impose Dirichlet displacement boundary conditions in small strain elasticity as well as the symmetric rotational boundary conditions for Kirchhoff-Love plates. The

skew-symmetric formulation is parameter-free in this context and achieves good accuracy: for the circular patch test we observe the predicted optimal convergence rates (Figure (7)).

• For patch coupling in statics, the skew-symmetric Nitsche formulation is still parameter-free. Condition numbers for the global stiffness matrix are far better than for standard Nitsche, and only slightly above the conforming setting. They are also almost independent of h, p and q: see Table (2) in Section 4.2.1.

• For patch coupling in modal analysis, Nitsche's formulation increases the number of 'outlier' frequencies. The reason is believed to be that Nitsche's formulation introduces additional highly localized eigenmodes, and the positions of these newly added eigenmodes just locate at the coupled interfaces.

• For contact problems in linear elasticity, the skew-symmetric Nitsche formulation behaves more robustly than the standard Nische formulation regarding the contact surface element length ratio, the number of quadrature points per element, and the value of γ. The Nitsche's method can properly impose the contact conditions, and predict the pressure distribution with respect to the contact width as the mesh is refined.

Acknowledgments

Qingyuan Hu is funded by China Scholarship Council. Stéphane Bordas thanks the financial support of the European Research Council Starting Independent Research Grant (ERC Stg grant agreement No. 279578). Stéphane Bordas is also grateful for the support of the Fonds National de la Recherche Luxembourg FNRS-FNR grant INTER/FNRS/15/11019432/EnLightenIt/Bordas. Franz Chouly thanks Région Bourgogne Franche-Comté for funding ("Convention Région 2015C-4991. Modèles mathématiques et méthodes numériques pour l'élasticité non-linéaire"), as well as the Centre National de la Recherche Scientifique ("Convention 232789 DEFI InFIniTI 2017 - Projet MEFASIM").

References

[1] T. J. Hughes, J. A. Cottrell, Y. Bazilevs, Isogeometric analysis: CAD, finite elements, nurbs, exact geometry and mesh refinement, Computer Methods in Applied Mechanics and Engineering 194 (2005) 4135–4195.

[2] L. Beirão da Veiga, A. Buffa, G. Sangalli, R. Vázquez, Mathematical analysis of variational isogeometric methods, Acta Numerica 23 (2014) 157–287.

[3] V. P. Nguyen, C. Anitescu, S. P. Bordas, T. Rabczuk, Isogeometric analysis: an overview and computer implementation aspects, Mathematics and Computers in Simulation 117 (2015) 89–116.

[4] R. N. Simpson, S. P. Bordas, J. Trevelyan, T. Rabczuk, A two-dimensional isogeometric boundary element method for elastostatic analysis, Computer Methods in Applied Mechanics and Engineering 209 (2012) 87–100.

[5] R. Simpson, S. Bordas, H. Lian, J. Trevelyan, An isogeometric boundary element method for elastostatic analysis: 2d implementation aspects, Computers & Structures 118 (2013) 2–12.

[6] M. A. Scott, R. N. Simpson, J. A. Evans, S. Lipton, S. P. Bordas, T. J. Hughes, T. W. Sederberg, Isogeometric boundary element analysis using unstructured T-splines, Computer Methods in Applied Mechanics and Engineering 254 (2013) 197–221.

[7] H. Lian, R. N. Simpson, S. Bordas, Stress analysis without meshing: Isogeometric boundary-element method, Proceedings of the Institution of Civil Engineers: Engineering and Computational Mechanics 166 (2013) 88–99.

[8] G. Beer, B. Marussig, C. Duenser, Isogeometric boundary element method for the simulation of underground excavations, Geotechnique letters 3 (2013) 108–111.

[9] B. Marussig, J. Zechner, G. Beer, T.-P. Fries, Fast isogeometric boundary element method based on independent field approximation, Computer Methods in Applied Mechanics and Engineering 284 (2015) 458–488.

[10] H. Lian, P. Kerfriden, S. Bordas, Implementation of regularized isogeometric boundary element methods for gradient-based shape optimization in two-dimensional linear elasticity, International Journal for Numerical Methods in Engineering 106 (2016) 972–1017.

[11] X. Peng, E. Atroshchenko, P. Kerfriden, S. Bordas, Isogeometric boundary element methods for three dimensional static fracture and fatigue crack growth, Computer Methods in Applied Mechanics and Engineering 316 (2017) 151–185.

[12] G. Xu, B. Mourrain, R. Duvigneau, A. Galligo, Parameterization of computational domain in isogeometric analysis: methods and comparison, Computer Methods in Applied Mechanics and Engineering 200 (2011) 2021–2031.

[13] G. Xu, B. Mourrain, R. Duvigneau, A. Galligo, Optimal analysis-aware parameterization of computational domain in 3D isogeometric analysis, Computer-Aided Design 45 (2013) 812–821.

[14] J. Kiendl, K.-U. Bletzinger, J. Linhard, R. Wüchner, Isogeometric shell analysis with Kirchhoff–Love elements, Computer Methods in Applied Mechanics and Engineering 198 (2009) 3902–3914.

[15] D. Benson, Y. Bazilevs, M.-C. Hsu, T. Hughes, Isogeometric shell analysis: the Reissner–Mindlin shell, Computer Methods in Applied Mechanics and Engineering 199 (2010) 276–289.

[16] D. Benson, Y. Bazilevs, M.-C. Hsu, T. Hughes, A large deformation, rotation-free, isogeometric shell, Computer Methods in Applied Mechanics and Engineering 200 (2011) 1367–1378.

[17] R. Echter, B. Oesterle, M. Bischoff, A hierarchic family of isogeometric shell finite elements, Computer Methods in Applied Mechanics and Engineering 254 (2013) 170–180.

[18] Q. Hu, Y. Xia, S. Natarajan, A. Zilian, P. Hu, S. Bordas, Isogeometric analysis of thin reissner-mindlin plates and shells: Locking phenomena and generalized local $\bar{B}$ method, arXiv preprint arXiv:1709.00402 (2017).

[19] V. P. Nguyen, T. Rabczuk, S. Bordas, M. Duflot, Meshless methods: a review and computer implementation aspects, Mathematics and Computers in Simulation 79 (2008) 763–813.

[20] C. Dunant, P. N. Vinh, M. Belgasmia, S. Bordas, A. Guidoum, Architecture tradeoffs of integrating a mesh generator to partition of unity enriched object-oriented finite element software, European Journal of Computational Mechanics/Revue Européenne de Mécanique Numérique 16 (2007) 237–258.

[21] I. Harari, J. Dolbow, Analysis of an efficient finite element method for embedded interface problems, Computational Mechanics 46 (2010) 205–211.

[22] I. Babuška, The finite element method with penalty, Mathematics of Computation 27 (1973) 221–228.

[23] N. Kikuchi, J. T. Oden, Contact problems in elasticity: a study of variational inequalities and finite element methods, volume 8 of *SIAM Studies in Applied Mathematics*, Society for Industrial and Applied Mathematics (SIAM), Philadelphia, PA, 1988.

[24] I. Babuška, The finite element method with Lagrangian multipliers, Numerische Mathematik 20 (1972/73) 179–192.

[25] C. Bernardi, Y. Maday, A. T. Patera, Domain decomposition by the mortar element method, in: Asymptotic and numerical methods for partial differential equations with critical parameters (Beaune, 1992), volume 384 of *NATO Adv. Sci. Inst. Ser. C Math. Phys. Sci.*, Kluwer Acad. Publ., Dordrecht, 1993, pp. 269–286.

[26] C. Bernardi, Y. Maday, A. T. Patera, A new nonconforming approach to domain decomposition: the mortar element method, in: Nonlinear partial differential equations and their applications. Collège de France Seminar, Vol. XI (Paris, 1989–1991), volume 299 of *Pitman Res. Notes Math. Ser.*, Longman Sci. Tech., Harlow, 1994, pp. 13–51.

[27] F. Ben Belgacem, The mortar finite element method with Lagrange multipliers, Numerische Mathematik 84 (1999) 173–197.

[28] B. I. Wohlmuth, A mortar finite element method using dual spaces for the lagrange multiplier, SIAM Journal on Numerical Analysis 38 (2000) 989–1012.

[29] E. Brivadis, A. Buffa, B. Wohlmuth, L. Wunderlich, Isogeometric mortar methods, Computer Methods in Applied Mechanics and Engineering 284 (2015) 292–319.

[30] I. Temizer, P. Wriggers, T. Hughes, Contact treatment in isogeometric analysis with NURBS, Computer Methods in Applied Mechanics and Engineering 200 (2011) 1100–1112.

[31] I. Temizer, P. Wriggers, T. Hughes, Three-dimensional mortar-based frictional contact treatment in isogeometric analysis with nurbs, Computer Methods in Applied Mechanics and Engineering 209 (2012) 115–128.

[32] L. De Lorenzis, P. Wriggers, G. Zavarise, A mortar formulation for 3D large deformation contact using nurbs-based isogeometric analysis and the augmented lagrangian method, Computational Mechanics 49 (2012) 1–20.

[33] J.-Y. Kim, S.-K. Youn, Isogeometric contact analysis using mortar method, International Journal for Numerical Methods in Engineering 89 (2012) 1559–1581.

[34] A. Seitz, P. Farah, J. Kremheller, B. I. Wohlmuth, W. A. Wall, A. Popp, Isogeometric dual mortar methods for computational contact mechanics, Computer Methods in Applied Mechanics and Engineering 301 (2016) 259–280.

[35] P. Antolin, A. Buffa, M. Fabre, A priori error for unilateral contact problems with lagrange multiplier and isogeometric analysis, arXiv preprint arXiv:1701.03150 (2017).

[36] J. Nitsche, Über ein Variationsprinzip zur Lösung von Dirichlet-Problemen bei Verwendung von Teilräumen, die keinen Randbedingungen unterworfen sind, Abhandlungen aus dem Mathematischen Seminar der Universität Hamburg 36 (1971) 9–15.

[37] R. Stenberg, On some techniques for approximating boundary conditions in the finite element method, Journal of Computational and Applied Mathematics 63 (1995) 139–148.

[38] R. Becker, P. Hansbo, R. Stenberg, A finite element method for domain decomposition with non-matching grids, ESAIM: Mathematical Modelling and Numerical Analysis 37 (2003) 209–225.

[39] P. Hansbo, Nitsche's method for interface problems in computational mechanics, GAMM-Mitteilungen 28 (2005) 183–206.

[40] C. Annavarapu, M. Hautefeuille, J. E. Dolbow, A robust Nitsches formulation for interface problems, Computer Methods in Applied Mechanics and Engineering 225 (2012) 44–54.

[41] A. Embar, J. Dolbow, I. Harari, Imposing Dirichlet boundary conditions with Nitsche's method and spline-based finite elements, International Journal for Numerical Methods in Engineering 83 (2010) 877–898.

[42] V. P. Nguyen, P. Kerfriden, M. Brino, S. P. Bordas, E. Bonisoli, Nitsche's method for two and three dimensional nurbs patch coupling, Computational Mechanics 53 (2014) 1163–1182.

[43] A. Apostolatos, R. Schmidt, R. Wüchner, K.-U. Bletzinger, A Nitsche-type formulation and comparison of the most common domain decomposition methods in isogeometric analysis, International Journal for Numerical Methods in Engineering 97 (2014) 473–504.

[44] M. Ruess, D. Schillinger, A. I. Özcan, E. Rank, Weak coupling for isogeometric analysis of non-matching and trimmed multi-patch geometries, Computer Methods in Applied Mechanics and Engineering 269 (2014) 46–71.

[45] Y. Guo, M. Ruess, Nitsche's method for a coupling of isogeometric thin shells and blended shell structures, Computer Methods in Applied Mechanics and Engineering 284 (2015) 881–905.

[46] X. Du, G. Zhao, W. Wang, Nitsche method for isogeometric analysis of Reissner-Mindlin plate with non-conforming multi-patches, Computer Aided Geometric Design 35/36 (2015) 121–136.

[47] W. Jiang, C. Annavarapu, J. E. Dolbow, I. Harari, A robust Nitsche's formulation for interface problems with spline-based finite elements, International Journal for Numerical Methods in Engineering 104 (2015) 676–696.

[48] K. Shahbazi, An explicit expression for the penalty parameter of the interior penalty method, Journal of Computational Physics 205 (2005) 401–407.

[49] E. Burman, A penalty-free nonsymmetric Nitsche-type method for the weak imposition of boundary conditions, SIAM Journal on Numerical Analysis 50 (2012) 1959–1981.

[50] S. Kollmannsberger, A. Özcan, J. Baiges, M. Ruess, E. Rank, A. Reali, Parameter-free, weak imposition of Dirichlet boundary conditions and coupling of trimmed and non-conforming patches, International Journal for Numerical Methods in Engineering 101 (2015) 670–699.

[51] T. Boiveau, E. Burman, A penalty-free Nitsche method for the weak imposition of boundary conditions in compressible and incompressible elasticity, IMA Journal of Numerical Analysis 36 (2016) 770–795.

[52] E. Burman, P. Hansbo, M. G. Larson, The penalty free Nitsche method and nonconforming finite elements for the Signorini problem, SIAM Journal on Numerical Analysis 55 (2017) 2523–2539.

[53] D. Schillinger, I. Harari, M.-C. Hsu, D. Kamensky, S. K. Stoter, Y. Yu, Y. Zhao, The non-symmetric Nitsche method for the parameter-free imposition of weak boundary and coupling conditions in immersed finite elements, Computer Methods in Applied Mechanics and Engineering 309 (2016) 625–652.

[54] F. Chouly, P. Hild, A Nitsche-based method for unilateral contact problems: numerical analysis, SIAM Journal on Numerical Analysis 51 (2013) 1295–1307.

[55] F. Chouly, An adaptation of Nitsche's method to the tresca friction problem, Journal of Mathematical Analysis and Applications 411 (2014) 329–339.

[56] F. Chouly, P. Hild, Y. Renard, Symmetric and non-symmetric variants of Nitsche's method for contact problems in elasticity: theory and numerical experiments, Mathematics of Computation 84 (2015) 1089–1112.

[57] Y. Guo, M. Ruess, D. Schillinger, A parameter-free variational coupling approach for trimmed isogeometric thin shells, Computational Mechanics (2016) 1–23.

[58] J. A. Cottrell, A. Reali, Y. Bazilevs, T. J. Hughes, Isogeometric analysis of structural vibrations, Computer Methods in Applied Mechanics and Engineering 195 (2006) 5257–5296.

[59] A. Cazzani, F. Stochino, E. Turco, An analytical assessment of finite element and isogeometric analyses of the whole spectrum of timoshenko beams, ZAMM-Journal of Applied Mathematics and Mechanics/Zeitschrift für Angewandte Mathematik und Mechanik 96 (2016) 1220–1244.

[60] T. Horger, A. Reali, B. Wohlmuth, L. Wunderlich, Improved approximation of eigenvalues in isogeometric methods for

multi-patch geometries and neumann boundaries, arXiv preprint arXiv:1701.06353 (2017).

[61] J. A. Cottrell, T. J. Hughes, Y. Bazilevs, Isogeometric analysis: toward integration of CAD and FEA, John Wiley & Sons, 2009.

[62] G. Xu, E. Atroshchenko, S. Bordas, Geometry-independent field approximation for spline-based finite element methods, in: Proceedings of the 11th World Congress in Computational Mechanics.

[63] R. Mlika, Y. Renard, F. Chouly, An unbiased Nitsche's formulation of large deformation frictional contact and self-contact, Computer Methods in Applied Mechanics and Engineering 325 (2017) 265–288.

[64] J. Freund, R. Stenberg, On weakly imposed boundary conditions for second order problems, in: Proceedings of the Ninth International Conference on Finite Elements in Fluids, Venice, pp. 327–336.

[65] F. Chouly, M. Fabre, P. Hild, R. Mlika, J. Pousin, Y. Renard, An overview of recent results on Nitsche's method for contact problems, Lecture Notes in Computational Science and Engineering (2017). Proceedings of the UCL Workshop 2016 on Geometrically Unfitted Finite Element Methods and Applications. Editors: Stéphane Bordas, Erik Burman, Mats G. Larson and Maxim Olshanskii. To appear.

[66] V. Thomée, Galerkin finite element methods for parabolic problems, volume 25 of *Springer Series in Computational Mathematics*, Springer-Verlag, Berlin, 1997.

[67] I. Harari, E. Shavelzon, Embedded kinematic boundary conditions for thin plate bending by Nitsche's approach, International Journal for Numerical Methods in Engineering 92 (2012) 99–114.

[68] M. Fabre, J. Pousin, Y. Renard, A fictitious domain method for frictionless contact problems in elasticity using Nitsche's method, SMAI Journal of Computational Mathematics 2 (2016) 19–50.

[69] F. Chouly, R. Mlika, Y. Renard, An unbiased Nitsche's approximation of the frictional contact between two elastic structures, Numerische Mathematik (2018). To appear.

[70] B. Juettler, U. Langer, A. Mantzaflaris, S. Moore, W. Zulehner, Geometry + simulation modules: Implementing isogeometric analysis, Proc. Appl. Math. Mech. 14 (2014) 961–962. Special Issue: 85th Annual Meeting of the Int. Assoc. of Appl. Math. and Mech. (GAMM), Erlangen 2014.

[71] O. Zienkiewicz, R. Taylor, J. Zhu, 9-The patch test, reduced integration, and non-conforming elements, in: O. Zienkiewicz, R. Taylor, J. Zhu (Eds.), The Finite Element Method Set (Sixth Edition), Butterworth-Heinemann, Oxford, sixth edition edition, 2005, pp. 329 – 355.

[72] J. Chen, C. Li, W. Chen, A family of spline finite elements, Computers & Structures 88 (2010) 718–727.

[73] Y. Bazilevs, L. Beirao da Veiga, J. A. Cottrell, T. J. Hughes, G. Sangalli, Isogeometric analysis: approximation, stability and error estimates for h-refined meshes, Mathematical Models and Methods in Applied Sciences 16 (2006) 1031–1090.

[74] J. N. Reddy, Theory and analysis of elastic plates and shells, CRC press, 2006.

[75] C. Adam, S. Bouabdallah, M. Zarroug, H. Maitournam, Improved numerical integration for locking treatment in isogeometric structural elements. part II: Plates and shells, Computer Methods in Applied Mechanics and Engineering 284 (2015) 106–137.

[76] R. L. Taylor, P. Papadopoulos, On a patch test for contact problems in two dimensions, Nonlinear Computational Mechanics (1991) 690–702.

[77] L. De Lorenzis, J. Evans, T. Hughes, A. Reali, Isogeometric collocation: Neumann boundary conditions and contact, Computer Methods in Applied Mechanics and Engineering 284 (2015) 21–54.

[78] M. Crisfield, Re-visiting the contact patch test, International Journal for Numerical Methods in Engineering 48 (2000)

435–449.

[79] N. El-Abbasi, K.-J. Bathe, Stability and patch test performance of contact discretizations and a new solution algorithm, Computers & Structures 79 (2001) 1473–1486.

[80] P. Wriggers, G. Zavarise, A formulation for frictionless contact problems using a weak form introduced by Nitsche, Computational Mechanics 41 (2008) 407–420.

[81] G. Zavarise, P. Wriggers, U. Nackenhorst, A guide for engineers to computational contact mechanics, Conzorcio TCN, 2006.